Nanoparticle Surfaces Studied by Electrochemical NMR

P. K. Babu, E. Oldfield,* and A. Wieckowski*

Department of Chemistry, University of Illinois at Urbana-Champaign,Urbana, IL 61801, USA.

I. INTRODUCTION

Exploring various phenomena at metal/solution interfaces relates directly to heterogeneous catalysis and its applications to fuel cell catalysis. By the late 1980s, electrochemical nuclear magnetic resonance spectroscopy (EC-NMR) was introduced[1,2] as a new technique for electrochemical surface science.[3] (See also recent reviews[4,5] and some representative references covering NMR efforts in gas phase surface science.[6-8]) It has been demonstrated that electrochemical nuclear magnetic resonance (EC-NMR) is a local surface and bulk nanoparticle probe that combines solid-state, or frequently metal NMR with electrochemistry. Experiments can be performed either under direct *in situ* potentiostatic control, or with samples prepared in a separate electrochemical cell, where the potential is both known and constant. Among several virtues, EC-NMR provides an electron-density level description of electrochemical interfaces based on the Fermi level local densities of states (Ef-LDOS). Work to date has been predominantly conducted with 13C and 195Pt NMR, since these nuclei possess reasonable gyromagnetic ratios, ensuring adequate sensitivity. They also have a nuclear spin I = 1/2, which generally simplifies data interpretation, due to the absence of quadrupolar effects. It was

demonstrated, for instance, that the 13C NMR of chemisorbed CO on Pt nanoparticles yields information based on the Ef-LDOS for both 5σ and 2π* orbitals. On the other hand, ^{195}Pt NMR offers an electronic-level description of the metal surface, including information on 6s and 5d Ef-LDOS of Pt, and the variations of these orbitals with surface modifications (particle size effects, adsorption/deposition, electrode potential change, *etc*.).[4,5] Several years of active research by different research groups[1,2,9-26] have contributed to a detailed understanding of many critical issues involved in electrochemical surface science of nanoparticle electrodes, with and without adsorbates. Here, we review the results of our efforts in the EC-NMR field. A theoretical section is added as an Appendix, and includes a short description of the electron-nucleus interactions in metals, together with phenomenological models used for the analysis of EC-NMR data.

Because of difficulties associated with the low sensitivity of NMR spectroscopy, a typical high-field NMR instrument needs ~10^{18} - 10^{19} NMR active atoms, for example ^{13}C spins, to make a signal detectable within a reasonable time period. Since 1 cm^2 of a single crystal metal surface contains about 10^{15} atoms, at least 1 m^2 surface area of NMR active atoms is needed to meet the NMR sensitivity requirement. This can be met by working with large surface area samples, such as nanoparticle catalysts, including platinum black and practically all fuel cell supported catalysts. Usually, a few hundreds of milligrams of the sample is sufficient for a typical EC-NMR experiment. With such high surface area electrodes, the use of EC-NMR yields unique information on the Fermi level local density of states, on surface bonding and/or the molecular structure of adsorbates, as well as surface dynamics at electrode surfaces.

In NMR (see Appendix), a specific resonance position (a frequency) corresponds to a specific chemical environment (a structure). This frequency is the chemical shift (δ_{CS}) in a molecule or the Knight shift (*K)* in a metal.[27] The familiar chemical or orbital shift arises from the shielding of the external magnetic field at the nucleus by the otherwise quenched orbital angular momentum of the surrounding electrons, while the Knight shift is produced by hyperfine interactions between nuclei and electrons. This effect is specific to metals since only electron spins at the Fermi energy can be polarized and therefore create a non-zero spin density in an external magnetic field (the so-called Pauli paramagnetism).[27] Among metals, ^{195}Pt has the largest known Knight shift, -33700 ppm vs. H_2PtI_6. The Pt metal Knight shift

is negative because of the major contribution from Pt 5*d* electrons to the electronic density of states at the Fermi level. Since the Knight shift (and the Korringa relationship[27]), are determined by the finite and quasi-continuous nature of the Fermi level local density of states (E_f-LDOS), measuring the Knight shift represents one of the primary probes of electronic structure in metals, and of surface molecular bonding.

Besides the chemical and/or Knight shift, there are two other major observables: the spin-lattice relaxation time in the laboratory frame (T_1), and the spin-spin relaxation time (T_2). While the chemical and/or Knight shift contains essentially static structural information, the temperature and/or magnetic field dependence of the relaxation times, both T_1 and T_2, are related to the dynamics of the observed nucleus. T_1 measures the rate at which the spin system returns back to thermal equilibrium with its environment (the lattice) after a perturbation, while T_2 measures the rate of achieving a common spin temperature within the spin system. Both T_1 and T_2 provide exceptionally important information on motions, varying typically from the 10^{-9} sec to 10^{2} sec timescales.

Below, we provide EC-NMR results for both ^{195}Pt and ^{13}C. We show the ^{195}Pt NMR lineshape for Pt nanoparticles supported on conducting carbon and a layer-model deconvolution that describes the surface, subsurface, etc., structure of these materials. We also present data obtained with unsupported Pt particle electrodes, discuss the spatially-resolved oscillation of the E_f-LDOS in a Pt catalyst and demonstrate correlations between the Pt Knight shift and the electro-negativity of the adsorbates. In ^{13}C-NMR, the observed temperature dependence of the relaxation rates obeys the Korringa equation, implying metallic behavior, just as is found in alumina supported Pt catalysts.[28] But in EC-NMR, we also show that spectra can be obtained under potential control, and that the observed spectra are sensitive to applied potentials. We describe results that indicate a linear relation-ship between the platinum clean surface Fermi level local density of states and the Knight shift of a ^{13}CO adsorbate. Variations of the E_f-LDOS reflects changes in the Pt-CO chemisorption bond due to both surface modifications (such as particle size change, alloying, deposition and/or chemisorption) and electrode potential change.

II. EXPERIMENTAL

Pt surfaces are routinely characterized using cyclic voltammetry (CV), usually at a sweep rate of 20 mV/min, in a preparative electrochemical cell containing a platinum gauze counter electrode, a 1 M NaCl Ag/AgCl reference electrode, and a working electrode. A typical working electrode consists of supported or unsupported platinum catalyst particles (50 to 500 mg) contained within a platinum boat.[4] Measurements are generally carried out in 0.5 M H_2SO_4 solutions under a blanket of ultra pure argon. The cell potential is controlled by a PGP201 Potentiostat/Galvanostat manufactured by Radiometer. Such Pt nanoparticle electrodes (and also a Pd electrode[16]) yield cyclic voltammograms that display features in the hydrogen region, as well as in the surface oxidation and double layer regions, that are characteristic of polycrystalline Pt electrodes. This shows that such an assembly of Pt nanoparticles can be considered as a polycrystalline electrode under well-defined, uniform potential conditions.

In a typical experiment, the originally oxidized nanoparticle Pt surfaces are first reduced by holding the cell potential at 250 mV for 1 to 2 hours, until the current decreases to an insignificant level. Then, an adlayer of ^{13}C- or ^{15}N- [4,11] adsorbate is produced on the electrode surface. In the case of surfaces covered by CO, the CO adsorbate can be produced either from electrochemical dissociative chemisorption of (99%) 13C labeled methanol, or from direct ^{13}CO adsorption from CO-saturated media. The platinum sample, clean or covered by an adsorbate, together with a small portion (2-3 ml) of supporting electrolyte, is then transferred into a 10-mm diameter x 25-mm length tube and flame-sealed under reduced pressure, in a nitrogen atmosphere. In electrode-potential-controlled experiments, the sample is transferred to an NMR-electrochemical cell. Samples prepared in this way do not show any deterioration with time, and do not display any significant electrode potential change, the drift being ~10 mV in a few days. The experiments performed on these samples have yielded reproducible values for the chemical shifts and relaxation times at any time scale of interest to electrochemical studies, indicating that the electrochemical interfaces remain intact in the NMR sample tubes or EC-NMR cells.[2,9,11,16]

All NMR measurements have been carried out by using *home-built* NMR spectrometers equipped with either 3.5-inch bore 8.47 or 14.1 Tesla superconducting magnets (Oxford Instruments, Concord,

Massachusetts), Aries data acquisition systems (Tecmag, Houston, Texas), and using an Oxford Instruments CF-1200 cryostat. A Hahn echo pulse sequence ($\pi/2$—τ—π—τ—acquisition) with 16-step phase cycling to eliminate ringdown, is used for data acquisition. Typical $\pi/2$-pulse length are between 5 and 16 μs, depending on the particular sample. Chemical shifts for ^{13}C are given in ppm from tetramethylsilane (TMS) and for ^{195}Pt, the Knight shifts are reported with respect to H_2PtCl_6. Spin-lattice relaxation times are measured by using an inversion-recovery method for ^{13}C and a saturation-recovery for ^{195}Pt, followed by a Hahn-echo acquisition sequence.

III. RESULTS AND DISCUSSION

1. Selected Topics in ^{195}Pt-NMR

The ^{195}Pt NMR lineshape of a collection of Pt nanoparticles is extremely broad,[4,29] extending downfield some 4 kilogauss from the position of bulk platinum, 1.138 G/kHz, (Figure 1). This is because Pt atoms on an individual nanoparticle shell are in a different chemical environment than are those in other shells, and they resonate at a different NMR frequency. The spectra typically contain a feature on the low-field side (1.100 G/kHz), which arises from surface atoms (the frequency difference is magnetic field dependent and is about 2.5 MHz in a field of 8.5 Tesla). *Ab initio* theoretical calculations on a five-layer Pt (100) cluster have demonstrated that this surface shift must be due to a gradual drop in the *d*-like Fermi level local density of states on moving from the inside of the particle to the surface.[30] It is this distinguishable surface signal, which makes ^{195}Pt NMR of particular use in investigating the surface physics and chemistry of nanoscale platinum particles.

The ^{195}Pt NMR spectra in Figure 1 were obtained for a platinum sample having an average Pt particle diameter of 2.5 nm, supported on conducting carbon (Vulcan XC-72). Figure 1A is a spectrum of an as-received sample. A surface peak appears at 1.085 G/kHz, the same position as platinum oxide, indicating that the Pt particle surfaces are covered by an oxide species.[29] Clearly, the ability to detect Pt surface oxide species is one of the virtues of NMR spectroscopy in nanoparticle

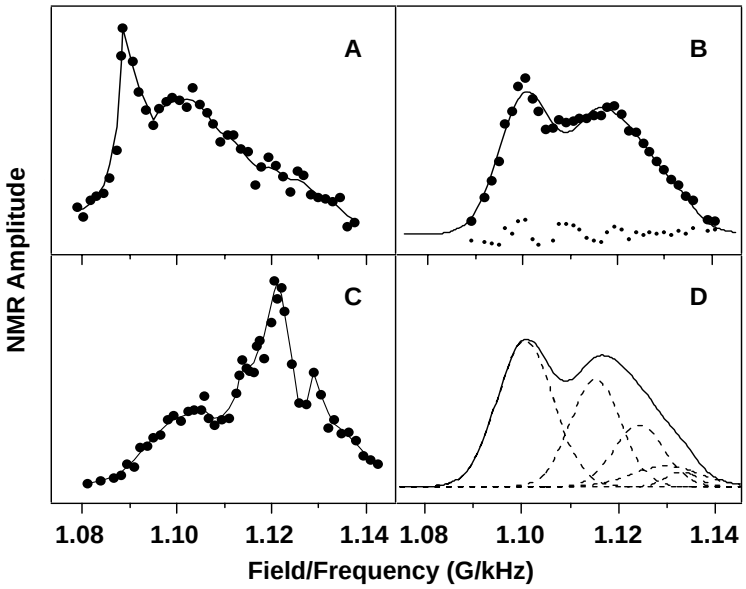

Figure 1. Point-by-point ^{195}Pt NMR spectra of 2.5 nm sample at T = 80K: A, As-received catalyst; B, electrochemically cleaned; C, sintered to nominally larger Pt size by extensive potential cycling and D, layer-model deconvolution of spectrum B. (Reprinted with permission from [15] Copyright 1999 Am. Chem. Soc.)

electrode surface characterization. (All Pt-type commercial nanoparticle catalysts come with their surfaces oxidized, which protect them from environmental contamination.) After electrochemical reduction of the same sample, done simply by holding the electrode at a potential within the double layer region,[9] one obtains the spectrum shown in Figure 1B (filled circles). Here, it is clear that the surface oxide peak disappeared giving rise to a new spectrum with the intensity near 1.100 G/kHz, attributable to the clean Pt surface,[29] and other spectral activity attributable to subsurface layers, or shells of platinum atoms (see below). The value of 1.100 G/kHz for the surface peak is to be compared to that of 1.138 G/kHz, which is assigned to bulk or core platinum atoms. Figure 1C also shows results obtained for 2.5 nm Pt particles after extensive voltammetric treatment, demonstrating pronounced sintering.[29]

The observations presented in Figure 1 are of interest since they show that, even when deposited on a conductive support and immersed in a liquid electrolyte, the small Pt particles show NMR properties typical of the same size particles deposited on non-conducting substrates,[31] or isolated in zeolites.[32] The fact that the Pt particles still retain a distinguishable surface peak also contrasts with the situation seen previously with self-supported Pt particles, where no surface peak was observed (Ref. [33], and see below). These surface properties were investigated in detail by using 195Pt NMR showing,[15,18,19,25] for example, a major enhancement of the surface E_f -LDOS in the electrochemical environment with respect to its gas phase counterpart.[34,35]

Figure 1 D presents the ^{195}Pt spectrum obtained using the layer model deconvolution technique (Appendix C).[15] From the deconvolution shown in Figure 1D, the fraction of Pt atoms in surface, subsurface and interior layers can be determined.[15] The average particle size (dispersion) can also be deduced from the lineshape since the surface signal is enhanced for smaller particles. Electronic structural information can be deduced from these lineshapes, using the *healing length* concept.[7] The healing length, defined as *m* times the distance between two consecutive layers (0.229 nm for Pt), is equal to 0.46 nm (≅ 2 Pt layers) for the sample shown in Figure 1D. This is to be compared with 0.31 nm (≅ 1.35 Pt layers) in the gas phase case,[36] indicating a significant change in the electronic structure of the Pt sample due to the presence of the double layer (as already mentioned above).[15] As reported previously, for larger nanoparticles, the contribution of the surface peak becomes reduced and, ultimately, may give way to the bulk Pt peak.[15] An example of this effect is shown in Figure 2 for carbon supported, electrochemically cleaned 3.2 nm nanoparticles. Although the surface peak is smaller than that on the 2.5 nm sample (Figure 1B), it is clearly distinguishable from other Pt atoms in the bulk of the nanoparticle.

2. Other Pt Nanoparticles (Unsupported and Supported)

Figure 3 shows the ^{195}Pt NMR spectrum of *unsupported* Pt-black samples, reduced electrochemically as reported above. The average particle size diameters are *ca*. 3 (Figure 3A) and 6 nm (Figure 3B), as

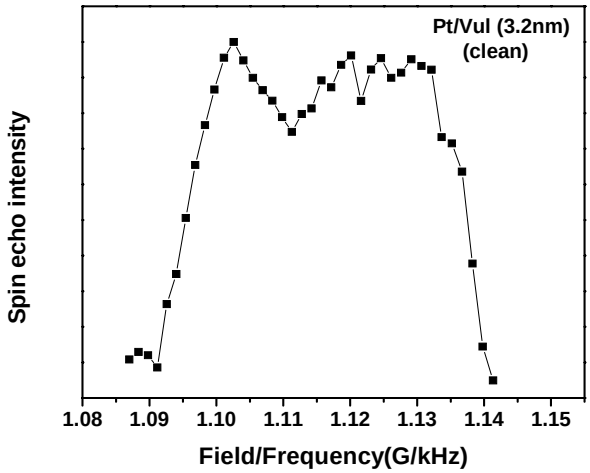

Figure 2. Point-by-point ^{195}Pt NMR spectra of 3.2 nm carbon-supported Pt nanoparticle after electrochemical cleaning.

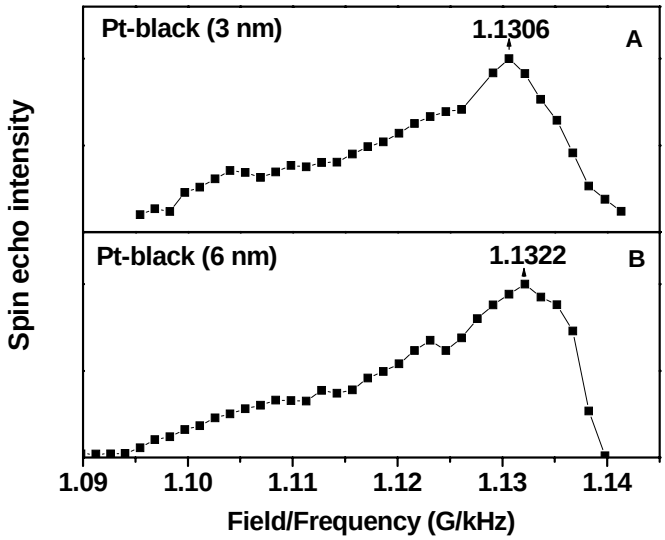

Figure 3. ^{195}Pt NMR spectra of unsupported Pt-black samples obtained point-by-point at T = 80 K in 8.45 T field (A) 3 nm (B) 6 nm.

obtained from TEM micrographs. Surface peaks (1.100 G/kHz) are absent, confirming previous results.[15] Nevertheless, a layer-like structure is certainly suggested since the spectra are spread over the range from 1.095 to 1.14 G/kHz, consistent with Pt atoms on the surface, sub-surface and interior layers, as described above. It is apparent, however, that the actual fraction of atoms that have a surface-like environment is quite low. An interesting observation can then be made concerning the peaks at 1.131 and 1.132 G/kHz for the smaller and larger particle sizes, respectively. Specifically, the frequencies of these peaks are much smaller than that reported for bulk Pt (1.138 G/kHz), which indicates that the smaller the particle size, the smaller the frequency of the *bulk* peak. Further modeling of such samples would be very useful since unsupported Pt nanoparticle samples are very active catalysts in fuel cells.[37]

3. Correlation Between the ^{195}Pt NMR Shift and Adsorbates Electronegativity

The influence of a series of different ligands or adsorbates (H, O, S, CN^-, CO, and Ru), adsorbed onto carbon-supported nanoscale Pt particles from the same starting batch has been investigated by ^{195}Pt NMR in an electrochemical environment.[19] The frequency difference between the resonance positions of the surface and bulk platinum atoms at 8.5 T is about 2.5 MHz, large enough to provide a convenient spectral visualization of how deep the influence of the adsorbate can go, as illustrated in the point-by-point ^{195}Pt NMR spectra (recorded at 80 K) presented in Figure 4. These spectra are normalized by equalizing their amplitudes at 1.131 G/kHz. Notice that only the Ru ligand yields a high frequency peak, which we will discuss in more detail elsewhere.[24] Another interesting observation is that the position of the high-field signal intensity (above 1.131 G/kHz), due to Pt atoms in the innermost layers, is independent of the type of the adsorbate. This adsorbate invariance provides direct experimental evidence for the validity of the Friedel-Heine invariance theorem,[38,39] which basically states that electronic properties at an atom, such as its LDOS, are determined primarily by the surrounding medium (to within a few electronic wavelengths). Although the chemical nature of the adsorbates is quite different, their influence on the LDOS is experienced by only those atoms on or very near the surface. That is, the high-field signals are invariant towards changes in surface electronic structure.

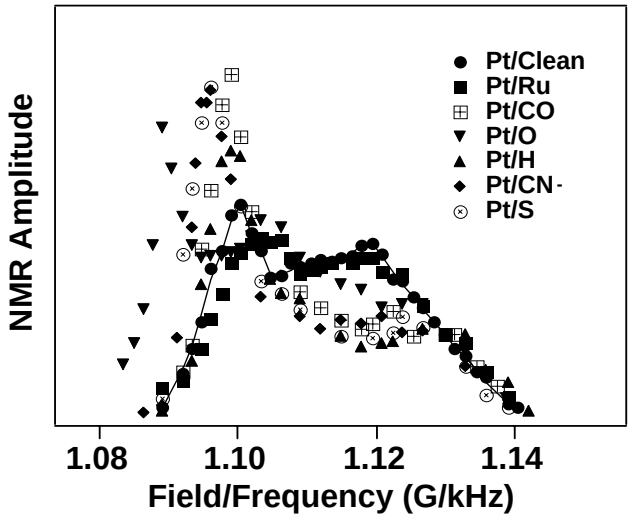

Figure 4. ^{195}Pt NMR spectra of 2.5 nm, carbon-supported Pt electrocatalyst with different adsorbates. The spectra are normalized by equalizing the amplitude at 1.131 G/kHz (indicated by the arrow). (Reprinted with permission from [19] Copyright 2000 *Am. Chem. Soc*.)

The changes induced by various adsorbates on the electronic properties of the electrode surface can be seen from the major frequency shift of the surface and subsurface NMR signals (Figure 5). The NMR layer model spectral deconvolution technique was applied to these spectra in order to obtain the variations in the surface and subsurface Knight shifts with surface adsorbate structure. The NMR parameters (such as peak position, width, relative intensity for the three central layers) were fixed to those of the clean-surface electrodes, while the surface and subsurface peak positions were allowed to vary. The results of these simulations are shown in Figure 5 and the surface and subsurface peak shift values obtained are plotted in Figure 6 as a function of the Allred-Rochow electronegativity. Allred-Rochow electronegativity is defined as the electrostatic force exerted by the nucleus on the valence electrons, expressed as:[40]

$$\chi_{AR} = \frac{3590Z^*}{r_c^2} + 0.744 \qquad (1)$$

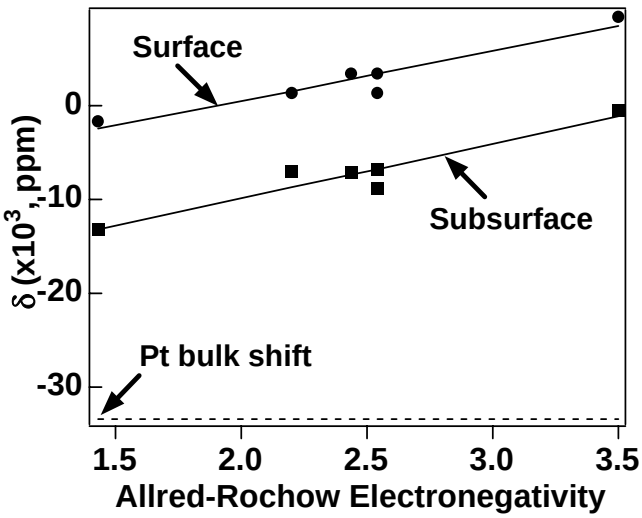

Figure 6. Correlation between surface/subsurface frequency shifts and the Allred-Rochow electronegativity of the adsorbates. The dashed horizontal line indicates the Knight shift of bulk platinum atoms. The solid straight lines are linear fits to the surface and subsurface shifts as a function of the electronegativity. (Reprinted with permission from [19] Copyright 2000 *Am. Chem. Soc*.)

where Z* is the effective nuclear charge seen by the valence electrons (obtainable from Slater's rule) and r_c is the covalent radius (pm). Tabulated values of the Allred-Rochow electronegativity of elements can be found in Ref [41].

Remarkably, both the surface and subsurface peak positions map almost linearly the electronegativity of the adsorbate. Also, the larger the electronegativity of the adsorbate, the longer the healing length; that is the deeper the influence of the adsorbate goes. It is also interesting to note that the value of *m* obtained for hydrogen adsorption (with the electronegativity $\chi = 2.2$) is about 2.9, very close to the *m* value (= 2.6) found by a detailed layer model analysis. In addition, for the adsorption of the alkali metal elements ($\chi \sim 1$), the prediction is that $m \sim 2$, virtually the same m as obtained for clean surface Pt particles in an electrochemical environment. One would, therefore, expect that alkali adsorption does not significantly change the ^{195}Pt NMR spectrum of

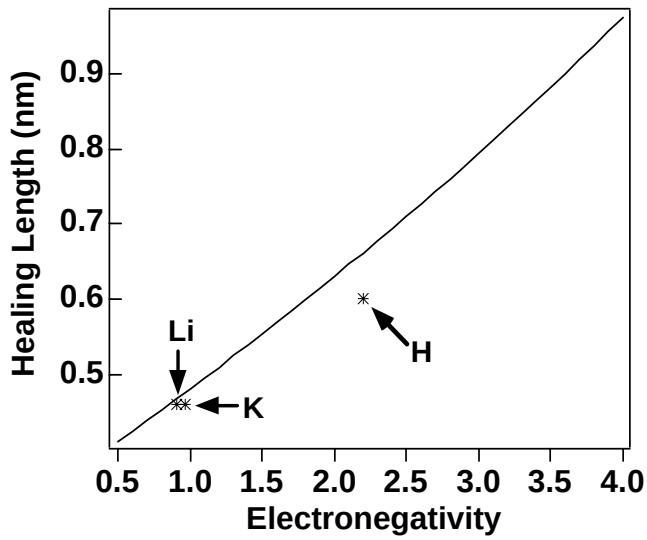

Figure 7. Healing lengths, estimated from the layer model analysis, plotted against the electronegativity. (Reprinted with permission from [19] Copyright 2000 Am. Chem. Soc.)

small Pt particles after adsorption. This is exactly what has been observed experimentally (in adsorption onto platinum from gas phase[42]). For comparison, these three experimentally estimated points are also plotted in Figure 7. (Note that the healing length values, obtained by multiplying 0.229 nm by *m*, are plotted in Figure 7 as a function of electronegativity, where 0.229 nm is the distance between two consecutive layers for Pt, see above.)

It is important to point out that the invariance observed here is in quite a different context to that of originally proposed in the Friedel-Heine invariance theorem, which refers to the invariance of electronic properties in bulk environments of dilute alloys. The situation is quite different for nanoscale metal particles from those of bulk Pt, due to the presence of the surface and the significant reductions in the particle volume. However, the E_f-LDOSs still show a remarkable invariance towards changes in surface chemical environment, even though they vary from those of bulk Pt. These results may also be expected to lead to useful general correlations between electronic properties and more

conventional chemical descriptions such as ligand electronegativity, which is helpful in understanding the electronic structure of metal/adsorbate interfaces.

4. Spatially-Resolved Oscillation of the E_f-LDOS in a Pt Catalyst

^{195}Pt NMR of nanoscale Pt particles can, in principle, permit a detailed study of the spatial variation of the E_f-LDOS across a given particle. This is possible because the ^{195}Pt NMR spectra are extremely broad and nuclei in individual platinum layers resonate at different frequencies, due to significant changes in local electronic properties caused by the presence of the particle's surface. The exponential healing model (Appendix C) relates the Knight shift of atoms at a given radial position to their distance from the surface, and such a spatial dependence provides the conditions necessary for the observation of indirect nuclear spin-spin *J*-coupling between neighboring Pt atoms as a function of radial position. Due to the large *J*-coupling that exists between neighboring Pt atoms, the spin echo decay curves exhibit a characteristic *slow-beat* pattern.[31] These spin echo decay measurements can be analyzed using a 5-parameter fit[31] to extract the *J*-coupling values.

We have carried out ^{195}Pt NMR investigations of (conducting) carbon-supported Pt nanoparticles having an average particle size of 8.8 nm, together with corresponding *J*-coupling measurements.[23] Figure 8 shows the Pt NMR spectrum of the clean sample. As above, Pt atoms in the interior have their resonances centered around 1.138 G/kHz and surface atoms give rise to a peak near 1.100 G/kHz. *J* values are determined from the spin echo envelopes at a series of spectral positions (Knight shifts). Figure 9 shows typical spin echo envelopes obtained across the spectrum, which can then be analyzed using the 5-parameter fit[31] to deduce the *J*-coupling values. The distance of each layer from the particle's surface can then be obtained by employing the exponential healing model. In a metal, the conduction electron mediated *J*-coupling is almost entirely determined by the *s*-like E_f-LDOS and it is proportional to $K_s(x)$, the Knight shift caused by *s*-like electrons at a position x away from the surface.[43] Assuming that local variations in $K_s(x)$ arise solely from variations in the *s*-like E_f-LDOS, one can readily deduce the following relationship[15] between the *s*-like E_f-LDOS, $D_s(E_f, x)$, and the *J*-coupling, $J(x)$, which enables a direct measurement of $D_s(E_f, x)$:

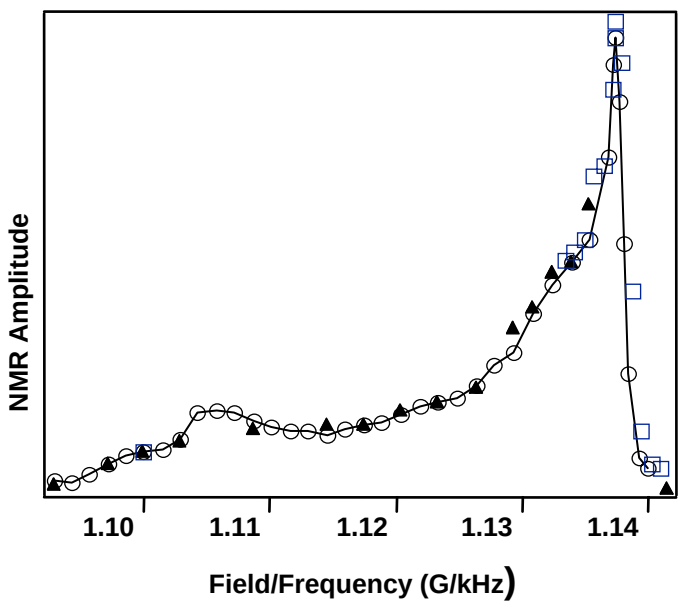

Figure 8. Point-by-point ^{195}Pt NMR spectrum of an 8.8 nm, carbon-supported clean surface Pt electrocatalyst. (After Tong *et al* [23] Copyright 2002, Elsevier Science Publishers)

$$D_s(E_f, x) = \left[0.098 + \frac{0.62}{J(x)}\right]^{-1} \tag{2}$$

The $D_s(E_f, x)$ values obtained from the *J*-coupling measurements are plotted as a function of *x* in Figure 10. It can be seen there that there is a clear oscillation in $D_s(E_f)$ across the spectrum. This represents the first experimental observation of a spatially-resolved oscillatory variation in $D_s(E_f)$ caused by the presence of a metal surface. Moreover, the experimental results can be fit to a simple relationship, which has the essence of a Bardeen-Friedel oscillation,[44]

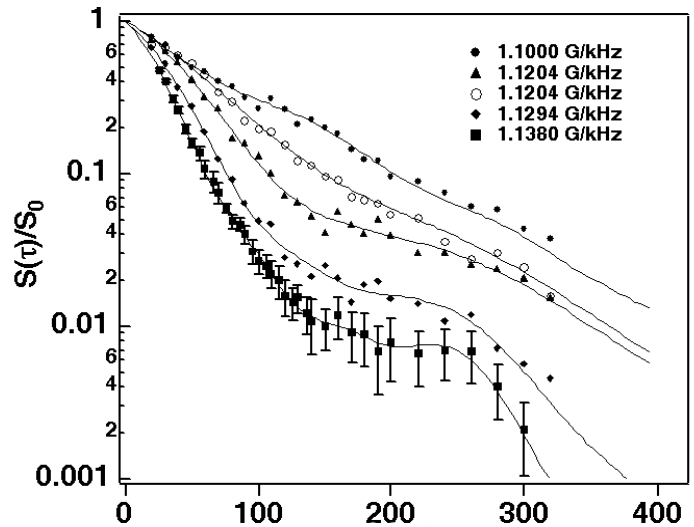

Figure 9. Spin-echo envelopes at different spectral positions, measured at 80 K for 8.8 nm, carbon-supported clean surface Pt electrocatalyst. Open symbols are from data measured from a reduced r.f. field strength. (After Tong *et al* [23] Copyright 2002, Elsevier Science Publishers)

$$D_s(E_f, x) = D_s(E_f, \infty) + b\frac{\sin(2k_F x)}{2k_F x} \tag{3}$$

The solid line in Figure 10 represents the fit to Eq. (3) which gives the following results: $D_s(E_f, \infty)$ = 3.5 atom^{-1}·Ry^{-1}, k_F = 6 nm^{-1}, and b = 1.5 atom^{-1}·Ry^{-1}. Notice that $\sin(2k_F x)/2k_F x$ is an asymptotic form of the oscillation but for simplicity, it is used here to approximate the behavior over the whole range. The value of $D_s(E_f, \infty)$, 3.5 atom^{-1}·Ry^{-1}, is very close to the accepted value for bulk Pt,[45] 4 atom^{-1}·Ry^{-1}. Assuming each Pt atom contributes one *s*-like electron, the *s*-like electron density for bulk Pt would be 6.1 x 10^{22}/cm^3. By following the simplest model for free electrons, one obtains k_F = 12 nm^{-1}, about twice the value we find. In other words, the value of 6 nm^{-1} for k_F indicates a much longer decay length than that would be expected from the Jellium model.[23] The oscillatory variation in $D_s(E_f)$ beyond 0.4 nm (Figure 10)

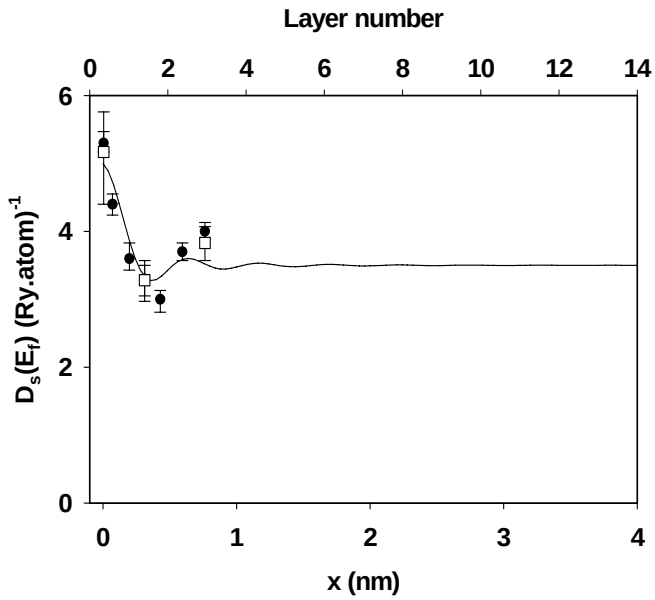

Figure 10. The s-like E_f -LDOS as a function of distance from the particle surface, showing oscillatory behavior. The solid line is a fit to Equation (3). (After Tong *et al* [23] Copyright 2002, Elsevier Science Publishers

indicates that the influence of the metal surface goes at least three layers inside the particles, in contrast to predictions based on the Jellium model. This conclusion is consistent, however, with the NMR results obtained for other nanoparticles and suggests that much of the observed broadening of the bulk-like peak in ^{195}Pt NMR spectra of such systems can be attributed to the spatial variation of the $D_s(E_f)$.

IV. ^{13}C NMR AT THE ELECTROCHEMICAL INTERFACE

1. ^{13}C NMR Knight Shift

An *ab initio* theoretical calculation shows that the rather localized 5σ HOMO and 2π* LUMO orbitals of CO before chemisorption become

extended bands after being chemisorbed onto a Pt(111) surface.[46] Before chemisorption, CO is non-metallic since there are no orbitals available at the Fermi energy, E_f. But upon interaction with the *d*-band of Pt(111), both 5σ and 2π* of CO on Pt(111) have orbitals available at E_f, *i.e.*, chemisorbed CO becomes metallic. This implies that for chemisorbed CO the Knight shift arises from conduction electrons in 5σ and/or 2π* orbitals.

In Figure 11, we show the ^{13}C NMR spectra of CO adsorbed on carbon-supported Pt nanoparticles with varying average sizes. The peak at ~160 ppm downfield from TMS can be assigned to ^{13}C present in the nonmetallic carbon support. The frequency shift of ^{13}CO adsorbed on platinum is at ~330 ppm from TMS, an approximately 170 ppm downfield shift from the 160 ppm values seen in many terminal or on top bonded diamagnetic metal carbonyls. This indicates the presence of a large Knight shift, *i.e.*, that the carbon atoms of CO the platinum surface are in the metallic state, as noted previously for CO on Pt in the gas phase (*i.e.*, in dry samples) by the Slichter group.[28]

As will be described in more detail in the Appendix, the Knight shift and the chemical shift are always measured together as a combined frequency shift. Fortunately, however, for CO adsorbed onto a metal surface, it is possible to use the Korringa relationship to detect the presence of conduction electrons and hence a Knight shift at the observed nucleus. The Korringa relationship indicates that $1/T_1 \propto T$, where T is the absolute temperature of the sample. In Figure 12, we show the relationship between the spin-lattice relaxation rates ($1/T_1$) of chemisorbed ^{13}CO (squares) and ^{13}CN (circles) on platinum.[4] The linearity of the ($1/T_1$) vs. T plot in chemisorbed CO and CN, respectively, and the Korringa products of T_1T = 82 s·K and 135 s·K, prove unambiguously that the carbon atom on the platinum surface in these two adsorbates is in a metallic state.

2. EC-NMR Under Potential Control

We found that the ^{13}C spectra of adsorbed CO and CN on Pt nanoparticle electrodes depend on the value of the electrode potential.[11,16] For EC-NMR under direct potential control, again, a few hundred milligrams of powdered Pt (fuel cell grade platinum black) was used as the working electrode in a three-electrode NMR electrochemical cell. The cell was positioned inside the NMR coil with the leads connected to an external potentiostat. The NMR electrochemical cell also incorporates

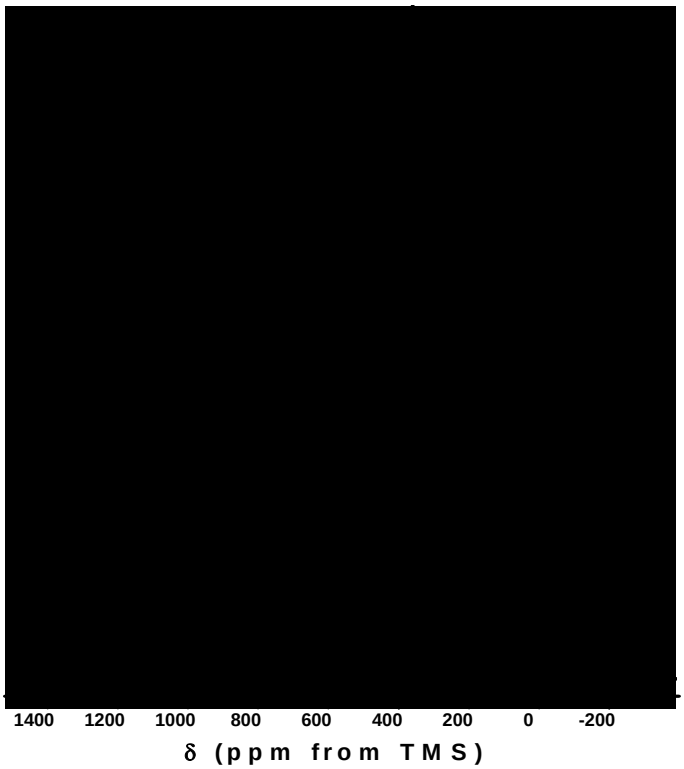

Figure 11. ^{13}C NMR spectra of chemisorbed CO on (A) 8.8 nm (B) 2.5 nm and (C) 2.0 nm particle size Pt-carbon samples (Reprinted with permission from [18]. Copyright 2000, Am. Chem. Soc.)

the ability to exchange the electrolyte without removing the probe from the magnet. CO was adsorbed onto the electrode surface by catalytic decomposition of ^{13}C enriched methanol. For CN^- adsorption studies, the 0.5 M H_2SO_4 was replaced by 0.5 M Na_2SO_4 adjusted to pH 11.2 with NaOH. A concentrated solution of ^{13}C-enriched sodium cyanide was then added to the basic solution to give a final concentration of 0.2 M CN^-. The adsorption of CN^- was carried out at -300 mV vs. a 3 M NaCl Ag/AgCl reference electrode. The data in Figure 13 demonstrate

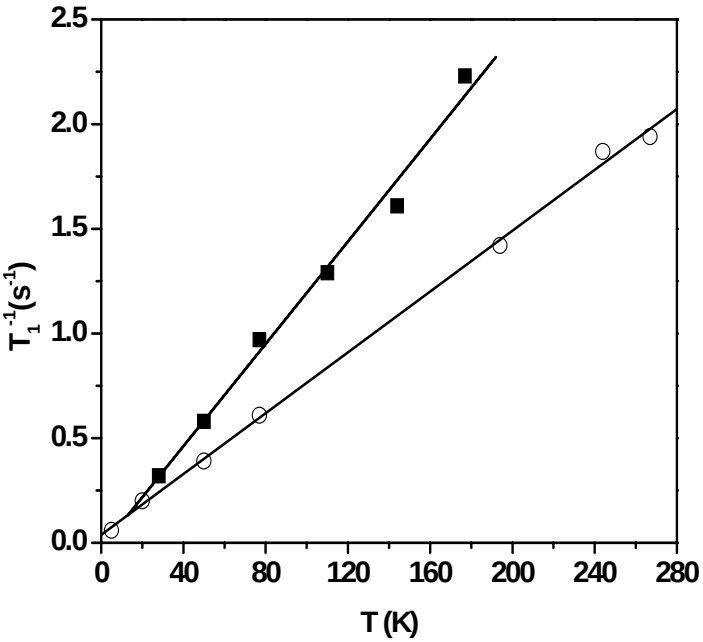

Figure 12. Temperature dependence of ^{13}C spin-lattice relaxation rate of adsorbed CO and CN on Pt black. (Reprinted with permission from [4]. Copyright 1998, Am. Chem. Soc.)

that ^{13}C resonances for both adsorbates became more shielded when the applied potential was increased in the positive direction, with the slope -71 ppm/V for ^{13}CO and -50 ppm/V for ^{13}CN. For CO on Pd, the slope was found to be even larger: about -136 ppm/V, as discussed below.[11]

3. Correlation of NMR to FTIR Data

In the field of FTIR of electrode surfaces, it is well known that the C–O vibrational frequency, ν_{CO}, decreases when the electrode potential becomes more negative. This variation of the vibrational frequency with electrode potential is referred to as the vibrational Stark effect.[47] The Stark effect can now be considered in the context of our NMR

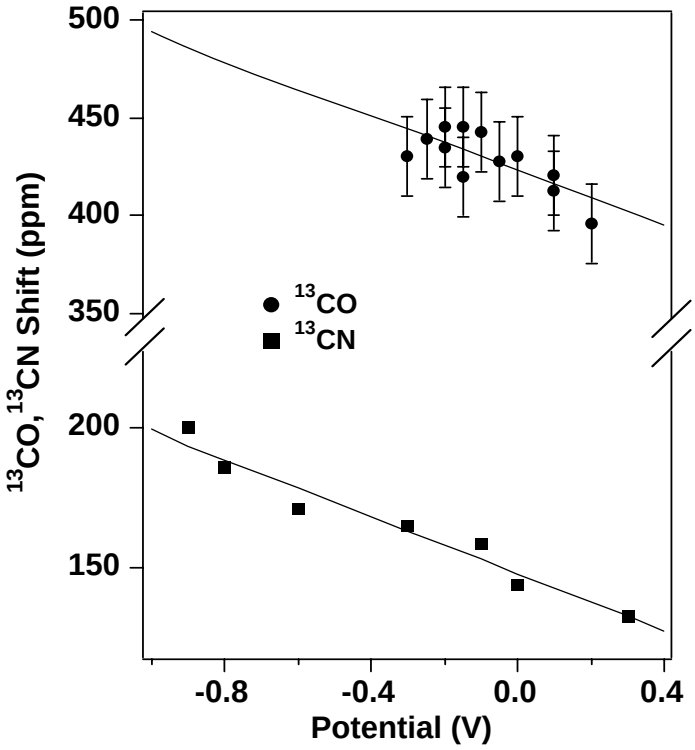

Figure 13. Potential dependence of the chemical shift of ^{13}CO and ^{13}CN adsorbed on Pt nanoparticles. (After Wu *et al* [11], Copyright 1997 Royal Society of Chemistry).

data. Here, we note that, first, the response of ^{13}C NMR to the electrode potential is due essentially to the Knight shift.[4,16] Second, the magnitude of the clean-surface E_f-LDOS of the Pt substrate correlates very well with the extent of the Knight shift as well as the vibrational stretch frequency of chemisorbed CO: the higher the clean surface E_f-LDOS, the larger is the ^{13}C Knight shift, or C–O stretch frequency of the CO. Both relationships are linear, with slopes of about 12 ppm·Ry·atom and -4 cm^{-1}Ry·atom respectively, giving a ratio of -3 ppm/cm^{-1}.[12,36] This is to be compared with the ratio of -2.8 ppm/cm^{-1}, obtained from the slopes (-71 ppm/V and 25 cm^{-1}/V respectively) of δ_{cs}

(^{13}C) in electrochemistry, and ν_{CO} versus electrode potential relationships for CO on Pt black. Third, variations in ν_{CO} can be directly correlated with changes in $2\pi^*$ back-donation: the higher the back-donation, the lower the CO stretch frequency. When taken together, all these observations suggest that the electrode potential dependence of both the ^{13}C NMR shift and the vibrational stretch frequency of adsorbed CO are primarily electronic in nature, and originate from changes in the E_f-LDOS at the metal surface and at the adsorbate, induced by electrode polarization.

4. Correlation Between Clean Surface E_f-LDOS of Metals and the Adsorbate Knight Shift

It is of interest to see if there exists any type of correlation between the clean surface E_f-LDOS of the metal and the ^{13}C Knight shift of chemisorbed CO. The former is an important surface attribute defining the ability of a metal surface to donate as well as to accept electrons, while the latter measures the degree of metallization of chemisorbed CO. Experimental data[15] for ^{13}C NMR of CO adsorbed onto 2.5 nm carbon-supported Pt particles and ^{195}Pt NMR of the corresponding clean metal surfaces were analyzed using the two-band models. Figure 14A shows the ^{195}Pt NMR spectra of a clean metal surface before and after CO adsorption. A typical relaxation recovery curve, measured at the surface peak (1.100 G/kHz) is shown in Figure 14B. A double-exponential fit (solid line) to the data gives the same relaxation times for the slow component before and after CO adsorption, indicating that the slow component arises from Pt atoms that are not bonded to CO. Therefore, relaxation data for the fast recovering component, from Pt atoms that are bonded to CO, can be analyzed with the two-band model.

A ^{13}C NMR spectrum of CO adsorbed onto 2.5 nm Pt particles is shown in Figure 15A.[15] The peak at 170 ppm again originates from the graphite support while the one at 380 ppm arises from CO adsorbed on platinum. For the adsorbed CO, the spin-lattice relaxation is found to be single exponential (inset of Figure 15A). The purely orbital contributions (chemical shifts) for atop CO on Pt and on Pd were calculated by using density functional theory (DFT) on model $COPt_7$ and $COPd_7$ clusters in which CO sits atop the central metal atom, which is coordinated by the remaining six metal atoms (inset in Figure 15B). For $COPt_7$, a value of 160 ± 20 ppm from TMS was obtained, while for

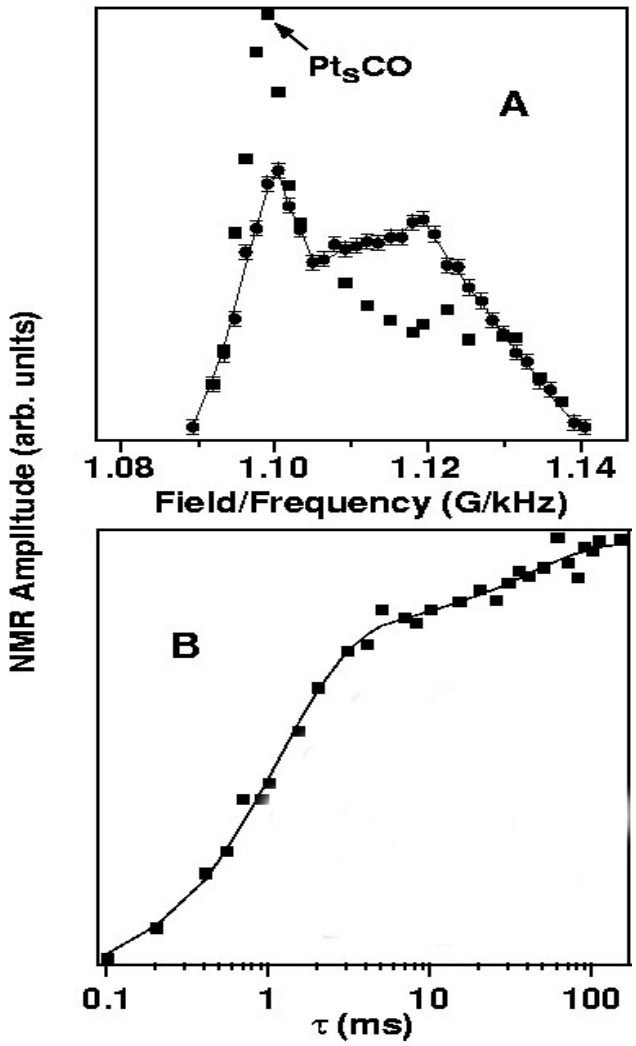

Figure 14. (A) Point-by-point ^{195}Pt NMR spectrum of clean Pt particles before and after CO adsorption, (B) Typical nuclear magnetization recovery profile for ^{195}Pt for the surface peak. The solid line is a two-exponential fit. (Reprinted with permission from [15] Copyright 1999 Am. Chem. Soc.)

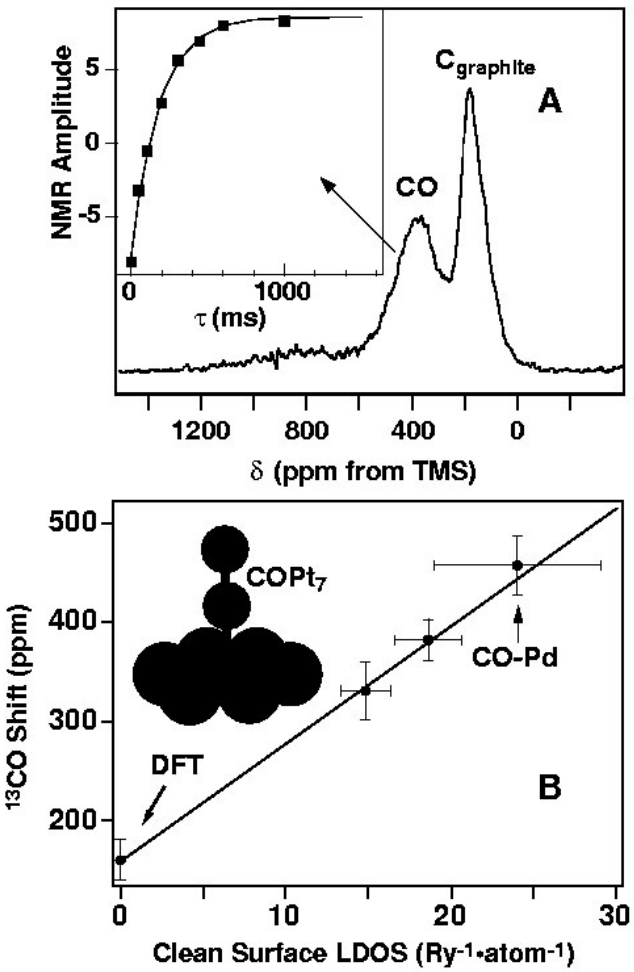

Figure 15. (A) ^{13}C NMR spectra of chemisorbed CO on Pt nanoparticles of size 2.5nm . Inset shows the magnetization recovery for ^{13}C of chemisorbed CO. (B) ^{13}C shift plotted as function of clean metal surface E_f-LDOS. Inset shows the 7-atom Pt cluster with adsorbed CO, used for the DFT calculations. (Reprinted with permission from [15] Copyright 1999 Am. Chem. Soc.)

$COPd_7$, the value was 203 ± 20 ppm. These calculated values are in surprisingly good agreement with available experimental data. The standard deviations account for uncertainties due to use of different functionals and basis sets. The clean surface E_f-LDOS for Pd was estimated based on the changes in magnetic susceptibility of small Pd particles with respect to their bulk value.

As may be seen in Figure 15B, the ^{13}C NMR shift of CO scales linearly with the clean surface E_f-LDOS before adsorption. A slope of 12 ppm·Ry·atom is obtained from the linear fit to the data. This linear relationship can be readily related to the frontier orbital interpretation of the Blyholder model.[48] A higher clean surface E_f -LDOS means more metal electrons and holes are available to engage in 5σ-forward and 2π*-back donation. As the E_f -LDOS increases, CO becomes more metallic, which results in a larger Knight shift. A very similar correlation to this has also been found to exist in the gas phase, where the C–O vibrational stretch frequency (after chemisorption) was shown to correlate linearly with the Pt clean surface E_f-LDOS before chemisorption.[12] The higher the surface E_f-LDOS, the lower the C–O stretching frequency. The linear relationship shown in Figure 15B is important because it demonstrates the validity of the frontier orbital-interaction picture of metal surface chemistry, where the importance of the clean surface E_f-LDOS is highlighted, in our electrochemical context. In addition, it puts ^{13}C NMR spectroscopic studies of chemisorbed CO on a firmer footing, by probing the electronic properties of transition metal surfaces before CO chemisorption.

4.5. NMR Comparison of CO Adsorbed on Pt-Black from Different Sources

^{13}C NMR of adsorbed CO on a metal nanoparticle electrode surface has been the main system investigated so far from the perspective of probing the properties of the Pt surface and Pt-CO interactions. In most of these NMR experiments, CO was chemisorbed onto metal nanoparticle catalyst surfaces through the catalytic decomposition of methanol. However, an ad-layer of CO can also be produced by immersing clean nanoparticles into electrolyte solutions saturated with CO. In order to understand whether the electronic properties of chemisorbed CO depended on the source from which it was chemisorbed, we have

carried out ^{13}C NMR experiments on CO chemisorbed onto Pt-black from methanol or from CO-saturated solutions.[49] CO was chemisorbed onto about 500 mg of catalyst from ^{13}C (99%) enriched CO solutions at open circuit. After 1 hour of adsorption, excess CO was removed by purging with argon and rinsing with 0.1 M D_2SO_4.

The ^{13}C EC-NMR spectrum of CO chemisorbed from the CO-saturated solution is shown in Figure 16A.[50] A single resonance peak around 370 ppm is found, basically as seen before in experiments where CO was generated from methanol. For comparison, the ^{13}C NMR spectrum of CO adsorbed via methanol oxidation is given in Figure 16B. The slight increase in the width of the NMR spectrum for CO chemisorbed from the gas phase may arise from the increased dipolar interaction between the CO molecules as a consequence of the higher CO coverage. The relaxation rates and their temperature

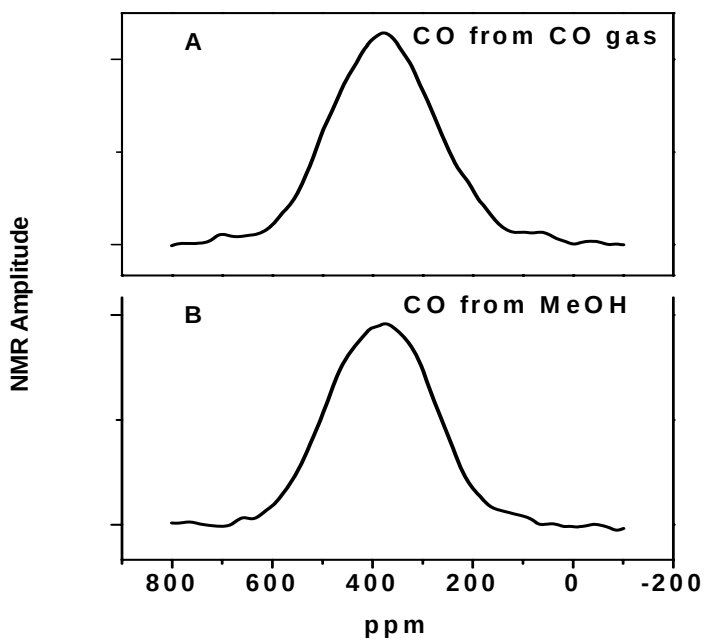

Figure 16. ^{13}C NMR spectra of CO adsorbed on clean Pt-black (A) CO generated from methanol oxidation (B) CO from CO gas (Reprinted with permission from [49] Copyright 2002 Am. Chem. Soc.)

Table 1
Comparison of the ^{13}C NMR Parameters of CO Produced from CO Gas and Methanol Oxidation on a Nanocrystalline Platinum Catalyst

	CO (From MeOH)	CO (From CO gas)
Peak (ppm)	370	375
T_1T (s.K)	59	57
$D_{5\sigma}(E_f)$ (Ry.atom)$^{-1}$	0.6	0.6
$D_{2\pi^*}(E_f)$ (Ry.atom)$^{-1}$	7.0	7.3

variation (see Table 1) are found to be essentially identical in both systems, implying that CO adsorbed on Pt has the same electronic properties irrespective of its source of generation. That is, the chemisorbed product from CO solutions and from methanol decomposition, are the same.

6. Effect of Surface Charge on the Chemisorption Bond: CO Chemisorption on Pd

The electrode potential dependence of the ^{13}C NMR spectra of CO adsorbed on Pd powder provides essential additional evidence for alterations to the metal/solution interface due to the application of an electric field.[4,16] Samples consisted of Pd powder with an average particle size of about 8 nm, produced by a gas condensation technique. Pd powder was cleaned in 0.1 M NaOH through multiple cycles of potential controlled reduction and oxidation. An adlayer of CO was produced from ^{13}CO saturating the supporting electrolyte. The cleaned powder and electrolyte were introduced into a sealed vessel and stirred under ^{13}CO gas.

The ^{13}C NMR spectrum of CO adsorbed on Pd is shown in Figure 17. CO adsorbed on Pd has a much larger Knight shift than CO on Pt (*c.f.*, for instance, Figure 16). This is attributed to a molecular orbital very near the Fermi level of Pd.[51] The peak position of the ^{13}C NMR spectrum shows a change as the electrode potential is varied and has a slope of -136 ppm/V. An estimate of the surface electric field was made from the IR stretching frequency of adsorbed CO to be about 10^9 V/m. A similar value is obtained from simple considerations of the

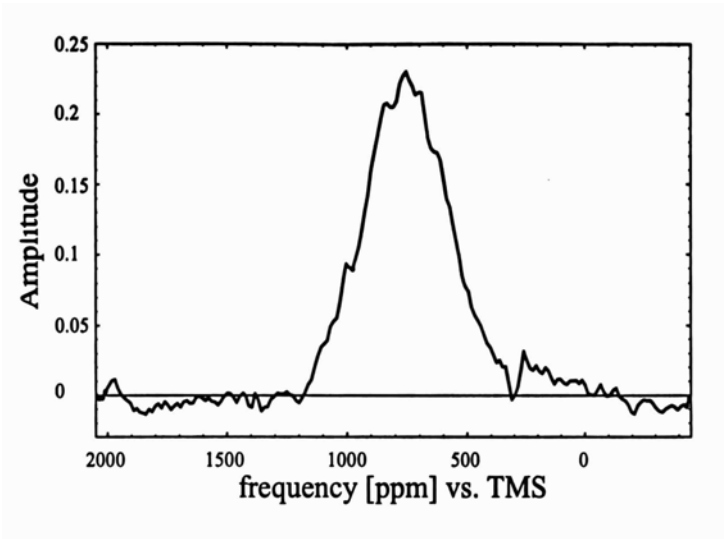

Figure 17. ^{13}C NMR spectrum of CO on Pd for a freshly prepared sample. (After Vuizzov *et al* [16] Copyright 1999, *Am. Phys. Soc.)*

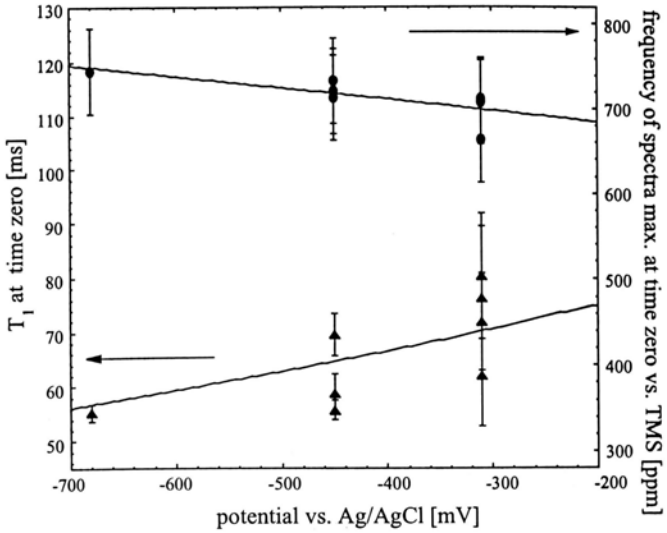

Figure 18. ^{13}C NMR line position (top) and spin-lattice relaxation time T_1 (bottom) of CO on Pd as a function of the electrode potential. (After Vuizzov *et al* [16] Copyright 1999, *Am. Phys. Soc*.)

measured capacitance. From the experimentally measured shift *vs*. electrode potential it was found that such electric fields could produce only about a –15 ppm/V change in the chemical shift. Therefore, it was concluded that the potential dependent NMR peak shift arises from changes in the Knight shift due to application of the electric field (see the above discussion for the Pt electrode). In addition, the potential dependence of the ^{13}C T_1 confirms this idea. Figure 18 shows both T_1 and the peak shift as a function of the applied potential. The straight line is a fit to the data with the T_1 values calculated using the Korringa relation (see above and Appendix). A good fit to both data sets is only obtained when the Knight shift is allowed to vary by the rate obtained above. Since the Knight shift is proportional to the E_f -LDOS, the changes in the Knight shift reflect the alteration to the E_f -LDOS by the electrode potential (or more specifically the electric field). Thus, EC-NMR under potential control serves as a prime tool to elucidate electronic changes in the electrochemical interface due to the presence of electric fields.

7. Pt Electrodes Modified by Ruthenium: A Study in Tolerance

Addition of Ru to Pt electrode surfaces is known to produce catalysts with enhanced CO tolerance. (For example, the CO stripping peak on Pt/Ru electrodes occurs at less positive potentials than on clean Pt electrodes.[52]) We have produced a series of Pt/Ru electrode surfaces using spontaneous deposition[22] of ruthenium onto commercial nano-particle platinum supports, and monitored their catalytic activity.[52] The spontaneous deposition method[37] used here, involves immersing platinum in a ruthenium chloride solution (in 0.1 M $HClO_4$), rinsing the sample in the cell with supporting electrolyte, then galvanically breaking the chemisorbed precursors to metallic/oxide ruthenium forms. Once a Pt surface decorated by metallic ruthenium is obtained in the first deposition, the deposition can be repeated many times in order to obtain the desired Ru packing density.[52] This method has several important advantages over other approaches: It is simple, yields active surfaces decorated by nano-sized islands of (predominantly) monatomic height and provides a good way for adjusting ruthenium coverage in the submonolayer deposition regime.

Results of methanol-electrooxidation reactivity measurements on four Pt/Ru samples (with Ru coverages of 0, 0.14, 0.35 and 0.53) are shown in Figure 19. The clean nanoparticle Pt electrode produces a

very small methanol oxidation current, due to severe CO poisoning. On the other hand, surfaces obtained by spontaneous deposition of ruthenium show enhanced tolerance to CO poisoning, and hence much higher steady-state currents. The extent of enhancement depends on ruthenium coverage (Figure 19), with maximum activity at a 0.4 - 0.5 fraction Ru packing density.[52] Two distinct CO stripping peaks can be seen (Figure 20) in the CV of the Pt/Ru samples, whereas for pure Pt black there is only a single peak, irrespective of CO coverage. This was the first observation of two CO stripping peaks on a bimetallic nanoparticle electrode. The total CO packing on the surface, obtained from CV, was estimated to be about 0.9 per metal surface site, indicating that CO is adsorbed on both Pt and Ru sites. Experimental results from Pt and Pt/Ru alloy electrodes[53] as well as numerical simulations[54]

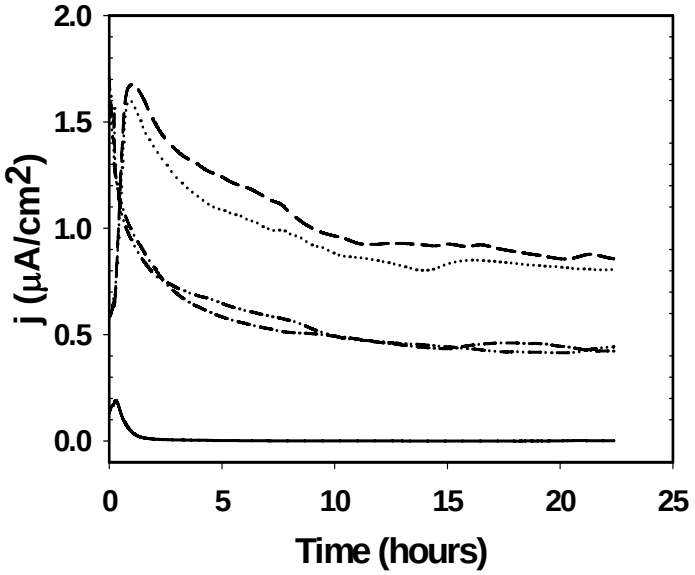

Figure 19. Methanol oxidation current density on Pt (—) and Pt/Ru: after 1st (—·—), 2nd (—··—), 3rd (····) and 4th (— —) deposition in 0.5 M methanol and 0.5 M H_2SO_4. Ruthenium packing density was 0.22, 0.23, 0.36, 0.40, respectively. (After Waszczuk *et al* [52] Copyright @2001 by Academic Press)

have shown that CO oxidizes at less positive potentials on Pt/Ru than it does on pure Pt electrode surfaces. Therefore, the low-potential CO stripping peak was assigned to CO adsorption on the Pt/Ru phase, and the higher potential peak, to CO adsorbed on Pt patches not occupied by ruthenium.[22,54-56] Notably, the results also show that progressively more CO's from the Pt phase are oxidized at low potential as the Ru coverage is increased.

In order to try to better understand the mechanism of enhanced CO tolerance, we undertook a ^{13}C NMR investigation of chemisorbed CO on these Ru modified electrode surfaces.[22] ^{13}C NMR spectra recorded in a 14.1 T magnetic field showed the presence of two broad peaks for

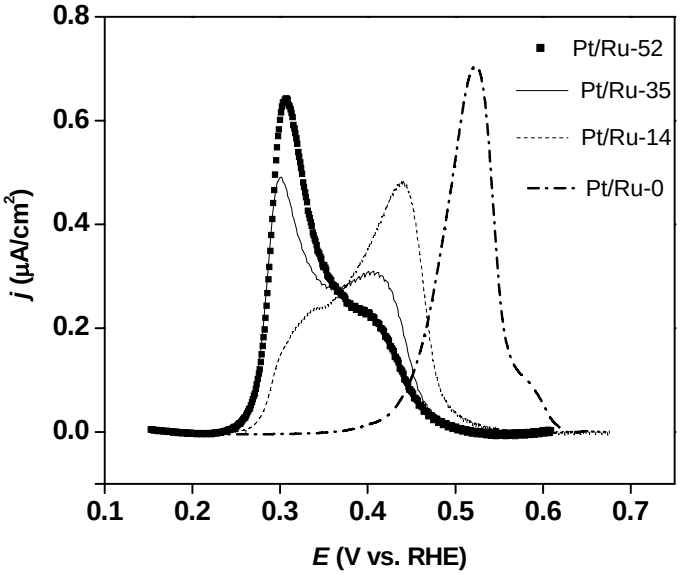

Figure 20. CO stripping from nanoparticle Pt/Ru electrode obtained at a scan rate of 10 mV s^{-1} after 12h of CO adsorption. With increasing Ru coverage, a new peak emerges to appear in the low potential region of the CV. (Reprinted with permission from [22] Copyright 2002 Am. Chem. Soc.)

each of several Pt/Ru samples (Figure 21) while only a single peak was seen for a pure Pt sample (Figure 16). Thus, EC-NMR also detects two CO populations: CO chemisorbed on pure Pt atoms and Ru atoms on the Pt/Ru electrodes, as was seen previously using infrared methods.[57-59] Since the electrochemical measurements suggest the presence of two CO domains (Pt, Ru/Pt) one can expect them to have different electronic properties. In fact, we were able to simulate the NMR spectra of a series of Pt/Ru samples using just two Gaussians. In Figure 21, we show such a double- Gaussian deconvolution of the NMR spectrum of one of these samples. Remarkably, the volume fractions of CO estimated from these NMR measurements are essentially identical to those obtained by CV, confirming the two-domain model proposed from the electrochemical measurements. The peak positions (obtained

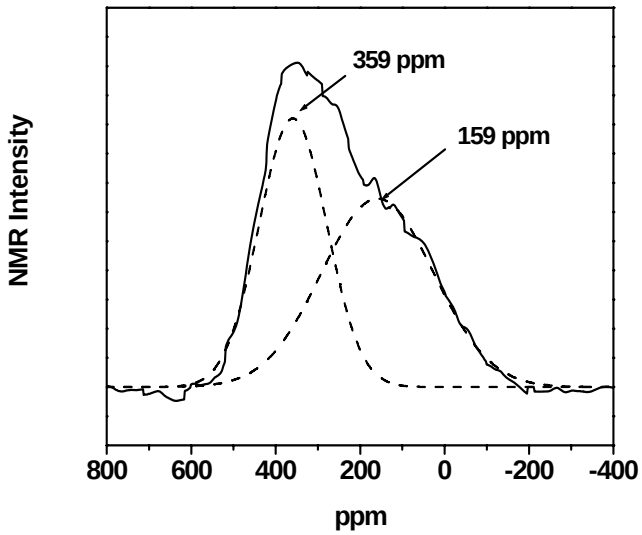

Figure 21. ^{13}C NMR spectrum of Pt/Ru-35 obtained in 14.1 T field. Dotted lines represent the double-Gaussian deconvolution that indicates the presence of two peaks, corresponding to the two different CO populations.

from deconvolution) and the spin-lattice relaxation data (measured at the two peak positions) are given in Table 2. The position of the low field peak changes by only 20 ppm as a function of Ru content. Also, the changes in the corresponding Korringa constants, T_1T, are relatively small. These results indicate that CO molecules resonating at low field,

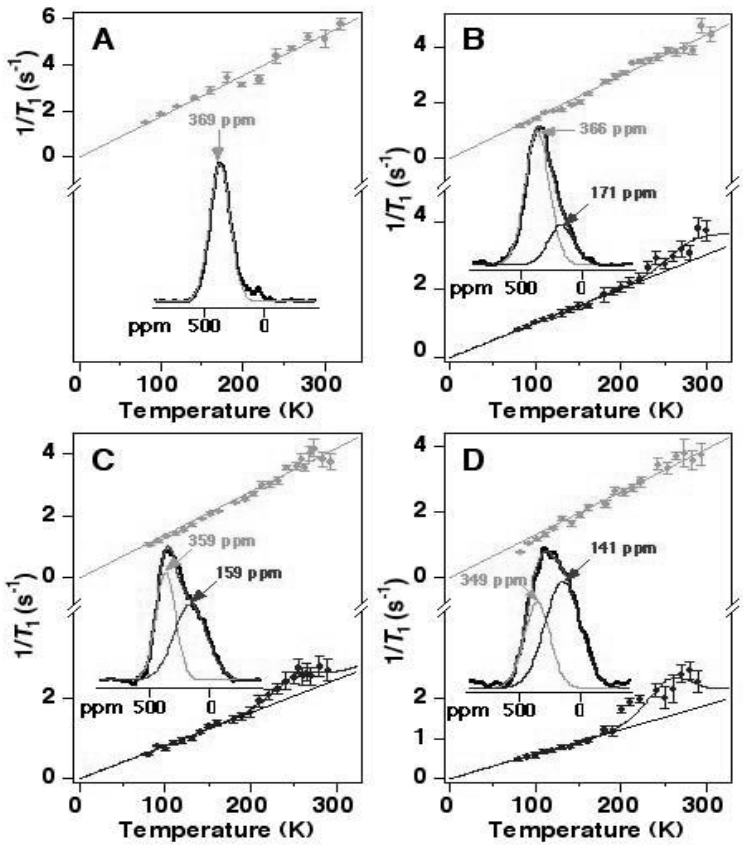

Figure 22. Temperature dependence of the ^{13}C nuclear spin-lattice relaxation rates for CO adsorbed on (A) Pt; (B) Pt/Ru-14; (C) Pt/Ru-35; (D) Pt/Ru-52. Insets show the double-Gaussian deconvolution. Relaxation rates are measured at the peak positions indicated by the arrows. (Reprinted with permission from [22] Copyright 2002 Am. Chem. Soc.)

Table 2
Double-Gaussian Deconvolution of ^{13}C NMR Data and the Corresponding T_1 Data.

		Pt/Ru-0	Pt/Ru-14	Pt/Ru-35	Pt/Ru-52
Low Freq.	Fraction	0	0.23	0.54	0.63
	peak (ppm)		171	159	141
	T_1T (s.K)		98	120	160
High Freq.	Fraction	1.00	0.77	0.46	0.37
	peak (ppm)	369	366	359	349
	T_1T (s.K)	59	67	71	75

assigned to CO bound to pure Pt regions, experience relatively weak electronic perturbations due to the presence of Ru. In sharp contrast, CO molecules resonating at high-field, assigned to COs bound to Ru islands, experience much stronger electronic perturbations. The high-field peak position (on the right) changes from 369 ppm (for pure Pt) to 141 ppm with increasing Ru coverage and is accompanied by a factor of 2 increase in T_1T.

More specific electronic and dynamic information about the nature of the metal-ligand interactions in these two domains can be obtained from temperature dependent nuclear spin-lattice relaxation measurements (Figure 22). For COs bound to pure Pt, the relaxation rate was found to follow the Korringa behavior throughout the temperature range (80-300K) examined whereas for the second species of CO, a diffusion-enhanced T_1 relaxation behavior was observed near room temperature. The solid lines in Figure 22A-D are fits to the following equation

$$T_1^{-1} = aT + \frac{2(\Delta\omega)^2\tau}{(1+\omega_0\tau^2)} \tag{4}$$

The first term is the standard Korringa contribution in which T is the absolute temperature and a^{-1} is the Korringa constant, obtained from the straight line fit at $T < 200$ K. The second term accounts for surface

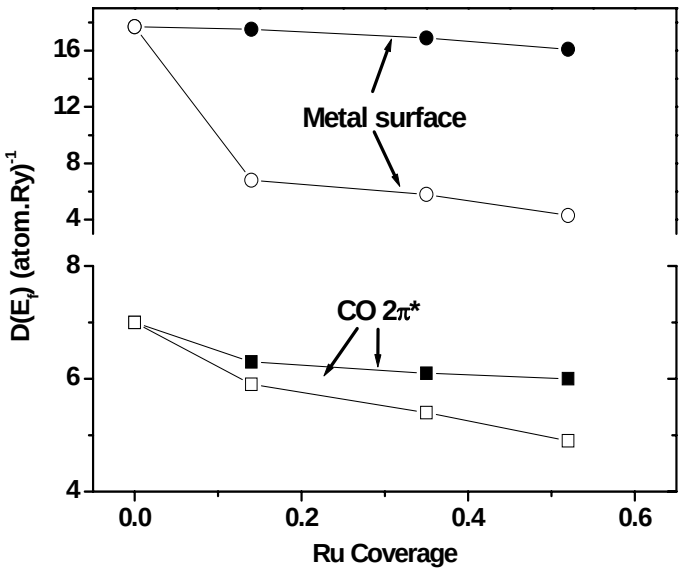

Figure 23. The metal surface E_f-LDOS before chemisorption and the 2π* E_f-LDOS at ^{13}C after chemisorption for (remote) Pt (solid symbols) and Pt/Ru (open symbols) sites, as a function of Ru coverage. (Reprinted with permission from [22] Copyright 2002 Am. Chem. Soc.)

diffusion, in which $\Delta\omega$ is the average local field inhomogeneity seen by a moving CO molecule, ω_0 is the NMR Larmor frequency, and τ is the correlation time. The correlation time is related to the activation energy for diffusion (E_{diff}) through the Arrhenius relation $\tau = \tau_0 \exp(E_{diff}/RT)$, where τ_0 is the preexponential factor, taken to be 10^{-13} s. The fit gives two parameters: the local field inhomogeneity $\Delta\omega$ and the activation energy for diffusion (E_{diff}). The values obtained for $\Delta\omega$ and E_{diff} are 3.3, 2.7, and 3.6 kHz and 5.7, 4.9, and 5.1 kcal/mol, for Pt/Ru-14, Pt/Ru-35, and Pt/Ru-52, respectively. For comparison, the activation energy for CO diffusion on pure Pt under the same electrochemical conditions has been previously determined to be 7.8 kcal/mol.[4,9,11] Clearly, the presence of Ru substantially enhances surface diffusion for the CO molecules on Pt/Ru sites, but for the Pt sites, the effects are very small. Thus, COs bound to Ru are more mobile than those adsorbed on Pt and

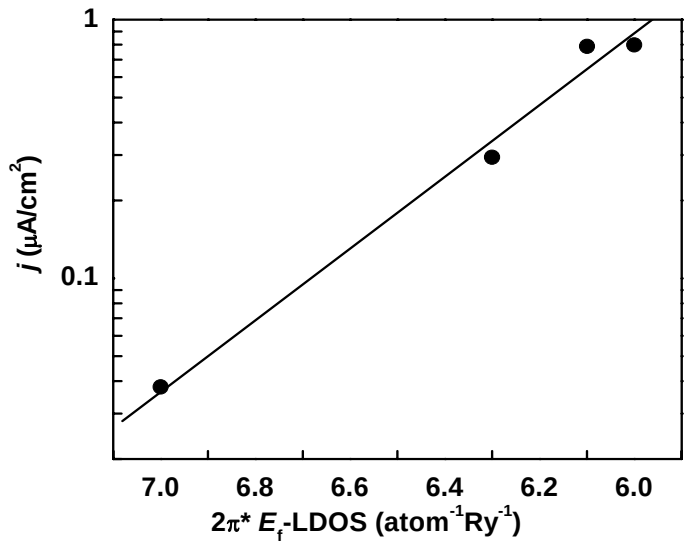

Figure 24. Graph showing the correlation between methanol oxidation current density (after reaching the steady-state) and $2\pi^*$ E_f-LDOS. (Reprinted with permission from [22] Copyright 2002 Am. Chem. Soc.)

there is no exchange between the two CO species, at least on this NMR time scale. Analyzing the spin-lattice relaxation data with the help of the two-band model, we then obtained the average Fermi level local density of states (E_f -LDOS) at the clean metal surfaces before chemisorption, and the $2\pi^*$- E_f -LDOS at ^{13}C after chemisorption (Figure 23). As Ru coverage increases, the clean metal E_f -LDOS decreases, causing a clearly discernable reduction in $2\pi^*$ back-donation, which weakens CO-metal bonding. Another interesting correlation can be seen when the methanol oxidation current density is plotted against the $2\pi^*$- E_f -LDOS, as shown in Figure 24. The oxidation current density shows a marked increase with the reduction in the $2\pi^*$- E_f -LDOS, clearly indicating the importance of electronic alterations in enhancing the CO tolerance of such Ru deposited catalysts.

From the EC-NMR data,[22] we conclude that diffusion of CO on Pt/Ru islands is fast and that the exchange between these two different

CO populations on the NMR and voltammetric timescale[22] is very slow. In summary, these observations demonstrate that there are two major populations of CO on Pt/Ru surfaces prepared by the spontaneous deposition method: COs located on Ru islands undergoing fast, thermally activated diffusion, and COs on Pt sites further away from Ru, undergoing slower diffusion.[4,11] With increasing Ru coverage, the E_f -LDOS for the clean metal surface and the $2\pi^*$ orbital of chemisorbed CO decrease, indicating there are strong electronic perturbations caused by the Ru addition. The increase in the catalytic activity of the Ru modified Pt nanoparticles appears to have a direct correlation with these electronic modifications.

8. EC-NMR of Pt/Ru Alloy Nanoparticles

As discussed above, Ru is an excellent promoter of Pt catalysts for methanol oxidation and Pt nanoparticles decorated with Ru show better performance in the oxidation process than do commercially available Pt/Ru (1:1) alloy nanoparticles.[22,52] In order to compare the electronic properties of these two systems, we undertook further ^{13}C NMR investigations of the Pt/Ru alloy nanoparticles covered by CO,[24] and have obtained new insights into the electronic alterations caused by Ru addition to Pt surfaces.

Cyclic voltammograms for CO stripping for the Pt/Ru alloy and commercial Pt black electrodes, obtained at a scanning rate of 10 mV/min, are shown in Figure 25. In the Pt/Ru alloy, the CO stripping peak is clearly shifted (as is well known) towards low potential, similar to the behavior seen previously with Pt black samples having Ru deposited through spontaneous deposition.[22] However, the two well resolved CO stripping peaks observed with the Ru-deposited samples (Figure 20) are now absent, Figure 25. Another interesting feature is that there is an increase in peak width for the Pt/Ru sample, suggesting that the Ru induces a broad range of local electronic structures in the Pt substrate, although unlike the situation with spontaneous deposition, the distribution is continuous rather than bimodal.

We show in Figure 26, the ^{13}C NMR spectra of CO adsorbed on Pt/Ru and Pt-black. For the alloy nanoparticles, Figure 26B, the whole spectrum has moved to a much lower overall shift (239 ppm) from TMS than that observed for CO on the Pt-black sample (375 ppm). In addition, there is a noticeable increase in the full-width at half-

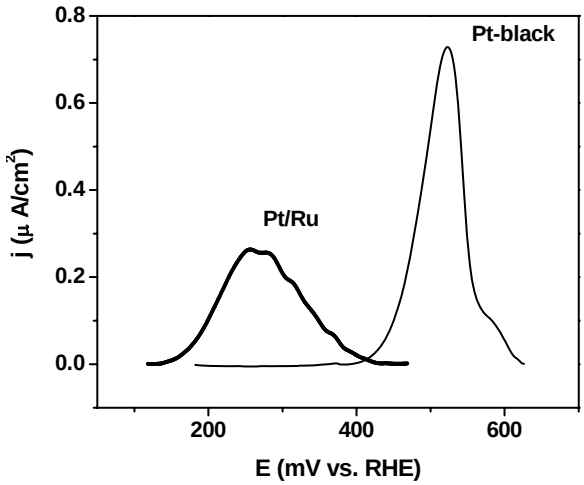

Figure 25. CO stripping voltammograms obtained after 12 hrs of methanol adsorption onto commercial Pt-black and Pt/Ru alloy nanoparticles. Scan rate was 10 mv/min. The surface areas are normalized.[24]

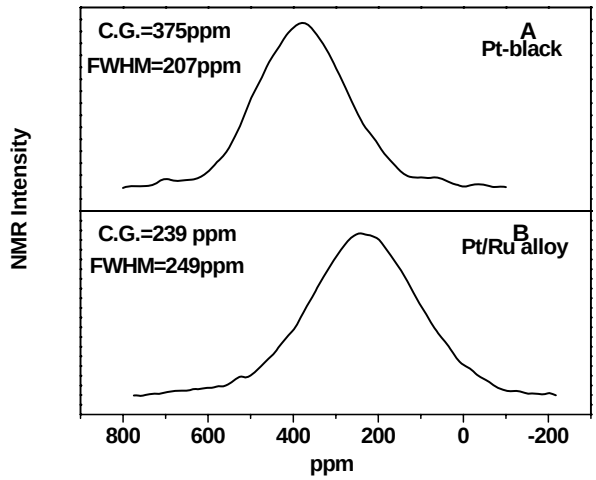

Figure 26. ^{13}C NMR spectra of chemisorbed CO on (A) clean Pt black and (B) clean Pt/Ru (1:1) commercial alloy nanoparticles. The FWHM changes from 207 to 249 ppm while the center of gravity shifts from 375 to 239 ppm as a result of Ru addition.[24]

maximum height (from 207 to 249 ppm). These results are consistent with the CV results. That is, in Pt black, the CV for CO stripping is narrow while that for the Pt/Ru alloy is broad, indicating a broad distribution of CO binding sites in the alloy, corresponding to different local Pt/Ru bonding environments (*e.g*. Pt/Ru compositional ratios, numbers of coordinating Ru atoms, Pt-Ru bond lengths). The actual shifts in the CV trace implies a weaker Pt-CO bond in the Pt/Ru alloy, consistent with the shift in the ^{13}CO NMR resonance (a low E_f -LDOS), due to a change in $2\pi^*$-back bonding. Moreover, the addition of Ru to Pt to form an alloy results in a downfield shift from the bulk Pt resonance position (1.138 to 1.106 G/kHz, see below), due to a decrease in the Pt E_f -LDOS. The decrease in overall ^{13}C shift of the adsorbed CO on the Pt/Ru alloy also implies that the E_f -LDOS of Pt atoms decreases due to the presence of Ru, consistent with the ^{195}Pt NMR results.

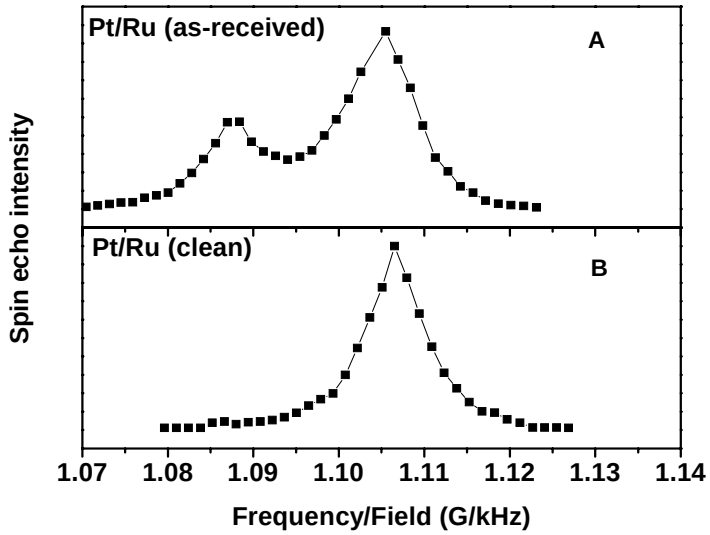

Figure 27. ^{195}Pt NMR spectra of commercial Pt-Ru (1:1) alloy, T = 80 K in 8.45 T field (A) As-received (B) Electrochemically cleaned.[24]

In Figure 27, we show the ^{195}Pt NMR spectra of an *unsupported*, commercial alloy (1:1) Pt/Ru catalyst obtained from Johnson-Matthey and having an average Pt particle diameter of 2.5 nm. The as-received material has a strong surface oxide peak (Figure 27A), which disappears after electrochemical reduction. The Pt NMR spectrum of the oxide-free Pt/Ru is completely different to that of the oxide-free and ruthenium-free Pt-samples discussed above, see Figure 1B. It consists of a symmetric, single Gaussian peak centered at 1.106 G/kHz, close to the pure Pt surface atom frequency. There are no Pt atoms resonating in the vicinity of 1.138 G/kHz, (the ^{195}Pt NMR bulk Pt frequency) and there are no subsurface peak characteristics of pure Pt particles either. Possibly, most Pt atoms are deposited on top of the nanoparticle, which has a dominant ruthenium (and/or ruthenium oxide[60]) core. More research is planned to test these ideas.

V. SUMMARY AND CONCLUSIONS

Clearly, ^{13}C and ^{195}Pt NMR form an ideal pair of non-invasive microscopic probes with which to investigate both sides of the electrochemical interface using electrochemical NMR. The results obtained by EC-NMR and reported in this review include the following. **In ^{195}Pt NMR**: (i) a layer-model analysis was applied for interpreting the ^{195}Pt NMR spectra of Pt nanoparticles supported on conducting carbon, (ii) spatially-resolved oscillations were found in the s-like Fermi level local densities of states (E_f -LDOS) of the Pt nanoparticles, and (iii) the ^{195}Pt NMR surface peak was demonstrated to be sensitive to the chemical nature of an adsorbate (a ligand). **In ^{13}C NMR studies**: (i) correlations were demonstrated between ^{13}C Knight shift of the CO adsorbate and E_f-LDOS of platinum, (ii) ^{13}C relaxation rates and their temperature variation were compared for CO deposited from methanol and from CO gas saturated solutions, (iii) the potential dependence of ^{13}C NMR spectra of CO adsorbed on Pt and Pd black was presented, and (iv) a two-band model was applied to the NMR shift and relaxation time to yield quantitative information about E_f -LDOS of Pt-CO surface chemical bonds, including data on the E_f -LDOS of both 5σ and $2\pi^*$ orbitals.

We believe we have given a fairly comprehensive account of the use of EC-NMR in electrochemical surface science and documented that EC-NMR provides information which cannot be obtained by any

other experimental method at a comparable level of detail, although in some cases the conclusions reached support previous work by XANES using synchrotron radiation.[61] Our results clearly demonstrate that due to a quantum mechanical electron density spillover from platinum, the interface is metallized, as evidenced by Korringa relaxation and Knight shift behavior. Thus, the adsorbate on a platinum electrode belongs to the metal part of the platinum-solution interface, and most likely other *d*-metal interfaces, and should be considered as such in any realistic models of the structure of the electrical double layer of interest to electrocatalysis.

We find that a layer model analysis can adequately describe the ^{195}Pt NMR spectrum of nanoscale electrode materials. The shifts of the surface and sub-surface peaks of ^{195}Pt NMR spectra correlate well with the electronegativity of various adsorbates, while the Knight shift of the adsorbate varies linearly with the E_f -LDOS of the clean metal surface. The ^{195}Pt NMR response of Pt atoms from the innermost layers of the nanoparticles does not show any influence of the adsorbate present on the surface. This provides experimental evidence, which extends the applicability of the Friedel-Heine invariance theorem to the case of metal nanoparticles. Further, a spatially-resolved oscillation in the *s*-like E_f -LDOS was observed via ^{195}Pt NMR of a carbon-supported Pt catalyst sample. The data indicate that much of the observed broadening of the bulk-like peak in ^{195}Pt NMR spectra of such systems can be attributed to spatial variations of the $D_s(E_f)$. The oscillatory variation in $D_s(E_f)$ beyond 0.4 nm indicates that the influence of the metal surface goes at least three layers inside the particles, in contrast to the predictions based on the Jellium model.

Comparing the results of EC-NMR and IR investigations, we find that the potential dependence of ^{13}C NMR shift and the vibrational frequency of adsorbed CO are primarily electronic in nature, and originate from changes in the E_f -LDOS. ^{13}C NMR results show that CO adsorbed on Pt, either directly from CO gas or from methanol oxidation, have the same electronic properties. That is, the chemisorbed product (surface CO) from CO solutions and from methanol decomposition is the same. The electrode potential dependence of the ^{13}C NMR spectra of CO adsorbed on Pt and Pd nanoparticles provide direct evidence for electric field induced alterations in the E_f -LDOS. In relation to fuel cell catalysis, EC-NMR investigations of Pt nanoparticles decorated with Ru show that there exist two different kinds of CO populations having markedly different electronic properties. COs

adsorbed on the Ru phase of Pt/Ru electrodes undergo faster diffusion and have a reduced E_f -LDOS, indicating that the CO-metal interaction is weakened due to the presence of Ru. The enhanced catalytic activity of Pt/Ru electrodes shows a direct correlation with the electronic alterations revealed by EC-NMR studies. Taken together, these results suggest that prospects for further studies are bright and indeed the method may have broader applications to improve our understanding of the electronic structure of electrochemical interfaces. Therefore, further utilization of this technique —with particular focus on electron-density level insights in to electrode adsorption and on studies of surface diffusion at electrochemical interfaces— may be expected.

VI. ACKNOWLEDGEMENTS

This work was supported by the Department of Energy Grants DEFG02-96ER45439 and DEGF-02-99ER14993, as well as by the National Science Foundation under Grant NSF CTS 97-26419.

VII. APPENDIX

1. Electron-Nucleus Interactions in Metal NMR

In NMR experiments, one observes the resonant absorption of electromagnetic radiation between nuclear spin energy levels are split due to the Zeeman interaction between the nuclear magnetic moments and the external magnetic field. However, this resonance frequency can be shifted from what one might expect due solely to the Zeeman interaction. In diamagnetic compounds shifts arises due to the interaction between the orbital magnetic moment of the electron with the nuclear spin. This is known as the chemical shift. In metals, in addition to this orbital interaction, it is possible to have a large perturbation of the electron spin magnetism due to the presence of conduction electrons. That is, since *s*-like conduction electron wavefunctions have finite overlap with the nuclei, there exists a strong interaction between the conduction electron and the nuclear spins, which leads to the Knight shift (K) in metals.

At thermal equilibrium, the nuclear spin energy levels are populated according to the Boltzmann distribution. Application of a radio frequency (RF) pulse that satisfies the resonance condition causes absorption of radiation and therefore, alteration in the spin population distribution. Thermal equilibrium populations are re-established when nuclear spins exchange their energies with the surroundings. This process is known as the nuclear spin-lattice relaxation and it is characterized by a time constant called T_1. T_1 is an important parameter whose numerical value and temperature dependence are characteristics of a material. In diamagnetic materials, molecular motions can produce the necessary fluctuating magnetic fields for the nuclear spin-lattice relaxation. In metals, electron-nuclear spin interactions that produce the Knight shift are often primarily responsible for the spin-lattice relaxation.

The Hamiltonian for the electron-nucleus interaction can be written as:

$$H = H_{FC} + H_D + H_{ORB} \tag{A1}$$

The first term is the Fermi-contact interaction given by

$$H_{FC} = \frac{8\pi}{3} \cdot \gamma_e \gamma_n \hbar^2 \mathbf{I} \cdot \mathbf{S} \delta(\mathbf{r}) \tag{A2}$$

where γ_e and γ_n are the gyromagnetic ratios of the electron and nuclear spins. **I** is the nuclear spin operator, **S** is the electron spin operator and $\delta(\mathbf{r})$ is the Dirac delta function, where **r** corresponds to the radius vector of the electron with the nucleus taken as the origin. Fermi-contact interaction causes a large shift in the NMR frequency of a nucleus compared to a diamagnetic reference. This interaction can scatter the conduction electrons near the Fermi level to vacant states by exchanging energy with nuclear spins, providing a very effective channel for nuclear spin-lattice relaxation. The energy associated with nuclear spin quanta is less than a micro electron-volt whereas a typical Fermi energy in metals is of the order of a few electron-volts. Since nuclear spin-lattice relaxation involves the conservation of energy, electrons can be scattered only to the vacant states that are lying very close to the Fermi level. In simple *s*-band metals, K and $1/T_1$ are related by the well-known Korringa equation:

$$T_1TK^2 = B\left(\frac{\gamma_e}{\gamma_n}\right)^2 \frac{\hbar}{4\pi k_B} \tag{A3}$$

where T is the absolute temperature and B is a constant, equal to unity when the many-body effects are negligible. This unique temperature dependence of $1/T_1$ is the NMR fingerprint of a metallic state. It results from the fact that only conduction electrons around the Fermi level can satisfy energy conservation for the electron-nuclear spin *flip-flop* relaxation process, and the fraction of these electrons is proportional to k_BT.

The second term of Eq. (A1) is the electron-nucleus dipole-dipole coupling and is given by

$$H_D = \gamma_e\gamma_n\hbar^2\mathbf{I.}\left(\frac{\mathbf{S}}{r^3} - \frac{3\mathbf{r(S.r)}}{r^5}\right) \tag{A4}$$

This dipolar interaction does not cause any shift in the NMR spectrum (or more precisely, the center of gravity). However, its time-dependent part can contribute to nuclear spin-lattice relaxation $[(1/T_1)_{\mathrm{dip}}]$. The third term of Equation (1), which represents the coupling of the orbital magnetic moment of the electron to the nuclear spin, is given by

$$H_{ORB} = \gamma_e\gamma_n\hbar^2\left(\frac{\mathbf{I.L}}{r^3}\right) \tag{A5}$$

where **L** is the orbital angular momentum of the electron. The isotropic part of H_{ORB} produces the chemical shift. In metals, the fluctuations in the orbital interaction could also contribute to the spin-lattice relaxation $[(1/\ T_1)_{\mathrm{orb}}]$. The Knight shift and the chemical shift are always measured together as a combined frequency shift, and there is practically no experimental distinction to be made between them. When δ_{CS} is of the same order as K, as with CO adsorbed onto a metal surface, one needs to use the Korringa relationship to confirm the presence of conduction electrons (and therefore of a Knight shift) at the observed nucleus.

B. Local Density of States and the Two-Band Model

In a typical EC-NMR experiment, the shift in the NMR frequency (K) and the nuclear spin-lattice relaxation time (T_1) are measured as function of temperature. The total shift in the NMR frequency consists of both the orbital part (K_{orb}) and the part due to the Fermi-contact interaction. For simple metals with only one type of electrons at the Fermi energy (E_f), the Knight shift is a function of the local density of states (LDOS) at E_f:

$$K \propto H_{hf}\, D(E_f) \tag{B1}$$

$$T_1 T K^2 = S \tag{B2}$$

where H_{hf} is the hyperfine field, $D(E_f)$ is the LDOS at the Fermi level and S is the Korringa constant appearing on the right hand side of Eq. (A3). The LDOS is defined by the following equation:

$$D(E_f) = 2\sum_i |\psi_i(\mathbf{x})|^2 \delta(E_i - E) \tag{B3}$$

where $|\psi_i(\mathbf{x})|^2$ is the probability of finding the ith electron with energy E_i at location **x**. The energy integral of the LDOS gives the total electron density at site **x**. In complex systems like the metal-adsorbate pair in EC-NMR, the LDOS at E_f can have contributions from more than one type of electron. For ^{195}Pt, there are contributions from 6*s* and 5*d* electrons, while for ^{13}C (in the chemisorbed CO) the LDOS at E_f consists of contributions from $2\pi^*$ and 5σ orbitals. In such cases, phenomenological two-band models[45.62] can be used to obtain the LDOS at E_f from the NMR parameters. For ^{195}Pt NMR, the total Knight shift can be written as

$$\begin{aligned} K &= K_s + K_d + K_{orb} \\ &= (1-\alpha_s)^{-1}\mu_B D_s(E_f) H_{hf,s} \\ &\quad + (1-\alpha_d)^{-1}\mu_B D_d(E_f) H_{hf,d} + \frac{\chi_{orb}}{\mu_B} H_{hf,orb} \end{aligned} \tag{B4}$$

and the Korringa relation becomes,

$$S(T_1T)^{-1} = k(\alpha_s)K_s{}^2 + k(\alpha_d)K_d{}^2R_d + (\mu_B D_d(E_f)H_{hf,orb})^2 R_{orb} \tag{B5}$$

where

$$k(\alpha) = (1-\alpha)\left(1+\frac{\alpha}{4}\right) \tag{B6}$$

For ^{13}C NMR of CO, the corresponding equations become,

$$\begin{aligned} K &= K_\sigma + K_\pi + K_{orb} \\ &= (1-\alpha_\sigma)^{-1}\mu_B D_\sigma(E_f)H_{hf,\sigma} \\ &\quad + (1-\alpha_\pi)^{-1}\mu_B D_\pi(E_f)H_{hf,\pi} + K_{orb} \end{aligned} \tag{B7}$$

and

$$S(T_1T)^{-1} = k(\alpha_\sigma)K_\sigma{}^2 + \left(\frac{1}{2}\right)k(\alpha_\pi)K_\pi{}^2 + \left(\frac{13}{5}\right)\left(\mu_B D_\pi(E_f)H_{hf,orb}\right)^2 \tag{B8}$$

In this formalism, the many-body effects are incorporated through the Stoner enhancement factor

$$\alpha_i = I_i\, D_i\,(E_f), \qquad i = s, d, \sigma, \pi \tag{B9}$$

and the Shaw-Warren de-enhancement factor $k(\alpha_i)$, where I_i is the exchange integral.[43] Using the parameters given in Table 1, it is possible to solve the set of simultaneous equations (for K and $S(T_1T)^{-1}$) to obtain $D_s(E_f)$, $D_d(E_f)$, $D_\sigma(E_f)$, and $D_\pi(E_f)$.

C. Layer Model Deconvolution and Exponential Healing

^{195}Pt NMR spectra of platinum nanoparticles are usually very broad, extending from 1.07 G/kHz to 1.138 G/kHz which corresponds to a range of almost 4 MHz at an 8.45 *T* field, which makes it is possible to distinguish NMR responses of surface Pt atoms from those of bulk and

other intermediate positions. The layer model deconvolution[36] is a very convenient method for analyzing ^{195}Pt NMR spectra of catalysts and takes into account the actual size distribution of particles. In this model, atoms in a nanoparticle sample are divided into groups belonging to various atomic layers. Particle size histograms obtained from transmission electron microscopy (TEM) are interpreted in terms of FCC cubooctahedra to estimate the fraction of atoms in each layer. Atoms from a given layer are assumed to produce a Gaussian NMR peak having a width of the order of one MHz. The observed NMR spectrum is then reconstructed by convoluting a set of Gaussians, each representing a given layer of the cubooctahedron. The peak position is taken as a function of the layer number[7] while their integrals are constrained to be proportional to the fraction of atoms in each layer. The widths of these Gaussians are taken as fitting parameters.

Particle size distribution histograms are constructed from the TEM micrographs by converting the image diameters (d_i) into the total number of atoms (N_T) in a particle using the following equation:

$$N_T = \pi \frac{\sqrt{2}}{6} \left(\frac{d_i}{2r_s} \right)^3 \tag{C1}$$

For platinum, $2r_s$ = 0.277 nm where r_s is the hard sphere radius. For each size distribution histogram obtained from the TEM, it is possible to find the number of cubooctahedral layers (l) by solving the equation

$$N_T = \left(\frac{10}{3} \right) l^3 - 5l^2 + \left(\frac{11}{3} \right) l - 1 \tag{C2}$$

The number of surface atoms in a given layer is calculated from,

$$N_S = 10l^2 + 20l - 12 \tag{C3}$$

The number of atoms in the subsurface layers is obtained by replacing l in Equation (C3) by (l - 1), (l − 2) and so on.

According to the *exponential healing theorem*,[7] the Knight shift of the n-th layer (K_n) heals back to the bulk value (K_∞), exponentially as a function of the layer number (n). Therefore, the Knight shift of the n-th layer can be written as

$$K_n - K_\infty = (K_0 - K_\infty)\exp(-n/m) \tag{C4}$$

where the dimensionless constant *m* is known as the *healing length* for the Knight shift.

VIII. REFERENCES

[1]K.W.H. Chan and A. Wieckowski, *J. Electrochem. Soc.* **137** (1990) 367.
[2]P.J. Slezak and A. Wieckowski, *J. Magnetic Resonance, Series A* **102** (1993) 166.
[3]A. *Interfacial Electrochemistry: Theory, Experiment, and Applications*, Ed. by A. Wieckowski, Marcel Dekker, New York, 1999.
[4]Y.Y. Tong, E. Oldfield, and A. Wieckowski, *Analytical Chemistry* **70** (1998) A 518.
[5]Y.Y. Tong, E. Oldfield, and A. Wieckowski, in: *Encyclopedia of Electrochemistry*: *Interfacial Kinetics and Mass Transport*, Vol. 2, Ed. E.J. Calvo, 2002.
[6]C.P. Slichter, *Ann. Rev. Phys. Chem*. **37** (1986) 25.
[7]J.J. Van der Klink, *Advances in Catalysis* **44** (2000) 1.
[8]Y.Y. Tong and J.J. van der Klink in*: Catalysis and Electrocatalysis at Nanoparticle Surfaces*, Ed. by A. Wieckowski, E. Savinova, and C. Vayenas, Marcel Dekker Inc., New York, 2002.
[9]J.B. Day, P.A. Vuissoz, E. Oldfield, A. Wieckowski, and J.P. Ansermet, *J. Am. Chem. Soc*. **118** (1996) 13046.
[10]M.S. Yahnke, B.M. Rush, J.A. Reimer, and E.J. Cairns, *J. Am. Chem. Soc.* **118** (1996) 12250.
[11]J.J. Wu, J.B. Day, K. Franaszczuk, B. Montez, E. Oldfield, A. Wieckowski, P.A. Vuissoz, and J.-P. Ansermet, *J. Chem. Soc. Faraday Trans.* **93** (1997) 1017.
[12]Y.Y. Tong, P. Meriaudeau, A.J. Renouprez, and J.J. van der Klink, *J. Phys. Chem. B* **101** (1997) 10155.
[13]C. Belrose, Y.Y. Tong, E. Oldfield, and A. Wieckowski, *Electrochem. Acta* **43** (1998) 2825.
[14]P.A. Vuissoz, J.-P. Ansermet, and A. Wieckowski, *Electrochem. Acta* **44** (1998) 1397.
[15]Y.Y. Tong, C. Rice, N. Godbout, A. Wieckowski, and E. Oldfield, *J. Am. Chem. Soc.* **121** (1999) 2996.
[16]P.A. Vuissoz, J.-P. Ansermet, and A. Wieckowski, *Phys. Rev. Letters* **83** (1999) 2457.
[17]C. Rice, Y. Tong, E. Oldfield, A. Wieckowski, F. Hahn, F. Gloaguen, J.M. Leger, and C. Lamy, *J. Phys. Chem. B* **104** (2000) 5803.

[18]Y. Y. Tong, C. Rice, A. Wieckowski, and E. Oldfield, *J. Am. Chem. Soc.* **122** (2000) 1123.
[19]Y. Y. Tong, C. Rice, A. Wieckowski, and E. Oldfield, *J. Am.Chem. Soc.* **122** (2000) 11921.
[20]B. M. Rush, J. A. Reimer, and E. J. Cairns, *J. Electrochem. Soc.* **148** (2001) A137.
[21]K. S. Han and O. H. Han, *Electrochimica Acta* **47** (2001) 519.
[22]Y. Y. Tong, H.-S. Kim, P. K. Babu, P. Waszczuk, A. Wieckowski, and E. Oldfield, *J. Am. Chem. Soc.* **124** (2002) 468.
[23]Y. Y. Tong, P.K. Babu, A. Wieckowski, and E. Oldfield, *Chem. Phys. Lett.* **361** (2002) 181.
[24]P. K. Babu, H. S. Kim, A. Wieckowski, and E. Oldfield, (2002) In Preparation.
[25]Y. Y. Tong, A. Wieckowski, and E. Oldfield, *J. Phys. Chem. B* **106** (2002) 2434.
[26]Y. Y. Tong, E. Oldfield, and A. Wieckowski, in*: Encyclopedia of Surface & Colloid Science*, Ed. by A. Hubbard, Marcel Dekker, Inc., 2002, p. 3713.
[27]C. P. Slichter, *Principles of Magnetic Resonance*, 3rd ed., Springer-Verlag, 1992.
[28]S. L. Rudaz, J.-P. Ansermet, P. K. Wang, and C. P. Slichter, *Phys. Rev. Lett.* **54** (1985) 71.
[29]Y. Y. Tong, C. Belrose, A. Wieckowski, and E. Oldfield, *J. Am. Chem. Soc*. **119** (1997) 11709.
[30]M. Weinert and A. J. Freeman, *Phys. Rev. B* **26** (1983) 6262.
[31]H. T. Stokes, H. E. Rhodes, P. K. Wang, C. P. Slichter, and J. H. Sinfelt, *Phys. Rev. B* **26** (1982) 3575.
[32]Y.Y. Tong, D. Laub, G. Schultz-Ekloff, A. J. Renouprez, and J. J. van der Klink, *Phys. Rev. B* **52** (1994) 8407.
[33]I. Yu, A. V. Gibson, E. R. Hunt, and W. P. Halperin, *Phys. Rev. Lett*. **44** (1980) 348.
[34]H. E. Rhodes, P. K. Wang, H. T. Stokes, C. P. Slichter, and J. H. Sinfelt, *Phys. Rev. B* **26** (1982) 3559.
[35]J.J. van der Klink, J. Buttet, and M. Graetzel, *Phys. Rev. B* **29** (1984) 11038.
[36]J. P. Bucher, J. Buttet, J. J. van der Klink, and M. Graetzel, *Surf. Sci*. **214** (1989) 347.
[37]P. Waszczuk, A. Crown, S. Mitrovski, and A. Wieckowski, in*: Fuel Cell Handbook: Fuel Cell Electrocatalysis*, Ed. by A. Lamm, H. Gasteiger, W. Vielstich, Wiley-VCH, in press.
[38]J. Friedel, *Adv. Phys*. **3** (1954) 446.
[39]V. Heine, Academic Press, New York, 1980; Vol. 35.
[40]A. L. Allred, E. G. Rochow, *J. Inorg. Nucl. Chem.* **5** (1958) 264.
[41]J. E. Huheey, *Inorganic Chemistry: Principle of Structure and Reactivity*, Harper Collins College Publishers, New York, 1993.
[42]Y. Y. Tong, G. A. Martin, and J. J. van der Klink, *J. Phys. Condens. Matter* **6** (1994) L553.

[43]J. J. van der Klink, and H. B. Brom, *Progress in Nuclear Magnetic Resonance Spectroscopy* **36** (2000) 89.
[44]R. L. Kautz and B. B. Schwartz, *Phys. Rev. B* **26** (1976) 2017.
[45]J. P. Bucher and J. J. van der Klink, *Phys. Rev. B* **38** (1988) 11038.
[46]B. Hammer, Y. Morikawa, and J.K. Nørskov, *Phys. Rev. Lett*. **76** (1996) 2141–2144.
[47]D. K. Lambert, *Electrochim. Acta* **41** (1996) 623.
[48]G. Blyholder, *J. Phys. Chem*. **68** (1964) 2772.
[49]C. Lu, C. Rice, R. I. Masel, P. K. Babu, P. Waszczuk, H. S. Kim, E. Oldfield, and A. Wieckowski, *J. Phys. Chem. B.* (2002) in press.
[50]P. K. Babu, Y. Y. Tong, H. S. Kim, and A. Wieckowski, *J. Electroanal. Chem.* 524-525 (2002) 157.
[51]J. Andzelm and D. R. Salahub, *J. Quantum Chem*. **29** (1986) 1091.
[52]P. Waszczuk, J. Solla-Gullon, H. S. Kim, Y. Y. Tong, V. Montiel, A. Aldaz, and A. Wieckowski, *J. Catalysis* **203** (2001) 1.
[53]H. A. Gasteiger, N. Markovic, P. N. Ross, Jr., and E.J. Cairns, *J. Electrochem. Soc*. **141** (1994) 1795.
[54]M. T. M. Koper, J. J. Lukkien, A. P. J. Jansen, and R. A. van Santen, *J. Phys. Chem. B.* **103** (1999) 5522.
[55]H. Massong, H. S. Wang, G. Samjeske, and H. Baltruschat, *Electrochem. Acta* **46** (2000) 701.
[56]G.-Q. Lu, P. Waszczuk, and A. Wieckowski, *J. Electroanal. Chem*. (2002) In Press.
[57]K. A. Friedrich, K. P. Geyzers, U. Linke, U. Stimming, and J. Stumper, *J. Electroanal. Chem*. **402** (1996) 123.
[58]W. F. Lin, M. S. Zei, M. Eiswirth, G. Ertl, T. Iwasita, and W. Vielstich, *J. Phys. Chem. B* **103** (1999) 6968.
[59]T. Iwasita, F. C. Nart, and W. Vielstich, *Ber. Bunsenegs. Phys. Chem*. **94** (1990) 1030.
[60]A. Crown, H. Kim, G. Q. Lu, I. R. de Moraes, C. Rice, and A. Wieckowski, *J. New Mat. Electrochem. Systems* **3** (2000) 275.
[61]J. McBreen and S. Mukerjee, in*: Interfacial Electrochemistry: Theory, Experiment, and Applications*, Ed. by A. Wieckowski, Marcel Dekker, New York, 1999, p. 895.
[62]J.J. van der Klink, *J. Phys.- Cond. Matt*. **8** (1996) 1845.